Int J Earth Sci (Geol Rundsch) (2006) 95: 703–723
DOI 10.1007/s00531-005-0052-8

ORIGINAL PAPER

J. Hladil · M. Gersl · L. Strnad · J. Frana
A. Langrova · J. Spisiak

Stratigraphic variation of complex impurities in platform limestones and possible significance of atmospheric dust: a study with emphasis on gamma-ray spectrometry and magnetic susceptibility outcrop logging (Eifelian-Frasnian, Moravia, Czech Republic)

Received: 6 August 2004 / Accepted: 4 September 2005 / Published online: 19 November 2005

Abstract Mineral dust and other constituents of Devonian atmospheric aerosols together with certain amounts of aquatic suspensions of riverine detrital origin, colloidal particle dispersions and seawater solutes were embedded in ~95–98% (or purer) limestones on a consistently subsiding isolated carbonate platform where they formed very complex impurity systems. Very low Th/U values, relative abundance of Fe but a slight excess of K typically characterize these ultrafine impurities which are mineralogically dominated by smectite–illite and mica (sericite) together with goethite. In vertical section, these impurities are arranged like incremental series of light and dense bands. The combined method of natural gamma-ray spectrometric and magnetic susceptibility measurements (GRS–MS) together with background of major and trace element analyses provided first systematic insights into fine-scale variability of these impurities in a pile of pure carbonate platform beds, mostly in inner platform *Amphipora* limestone facies. These carbonates were deposited close to sea level but far from river mouths, and they represented a certain sort of a relatively "independent" medium that was primarily sensitive to climatically (and by rare events) controlled input of atmospheric dust. A remarkable similarity of MS stratigraphic patterns that reflect the quantity and quality of embedded impurities in very distant and paleogeographically separated Devonian basins might be seen as supporting this viewpoint. A long composite stratigraphic section of the Moravian Karst ranges from mid-Eifelian to end-Frasnian levels and yields a number of time characterizing GRS–MS variations that can potentially serve as templates for high-resolution stratigraphic correlations over long distances.

Keywords Complex impurities · Platform limestones · Gamma-ray spectrometry · Magnetic susceptibility · Devonian

Electronic Supplementary Material Supplementary material is available for this article at http://dx.doi.org/10.1007/s00531-005-0052-8 and is accessible for authorized users.

J. Hladil (✉) · A. Langrova
Institute of Geology, Academy of Sciences CR,
Rozvojova 135, 165 02 Prague, Czech Republic
E-mail: hladil@gli.cas.cz
Tel.: +420-2-33087238
Fax: +420-2-20922670

M. Gersl
Czech Hydrometeorological Institute, Brno Branch,
Kroftova 43, 616 67 Brno, Czech Republic

L. Strnad
Laboratories of the Geological Institutes, Charles University,
Albertov 6, 128 43 Prague, Czech Republic

J. Frana
Institute of Nuclear Physics, Academy of Sciences CR,
250 68 Rez near Prague, Czech Republic

J. Spisiak
Geological Institute, Slovak Academy of Sciences,
Severna 5, 974 01 Banska Bystrica, Slovak Republic

Introduction

Previous studies

The detailed stratigraphic variation of impurities in limestones seems to be an attractive research topic in present-day high-resolution stratigraphy. The magnetic susceptibility (MS) stratigraphy as developed since the mid-1990s (e.g. Crick et al. 1997, 2001) cover many Paleozoic stage boundary sections with a field resolution of ~3–5 cm. This resolution typically relates to a few metres of condensed carbonate strata that deposited in conditions of slopes and toes with sedimentation rates of ~5–25 m/Ma. From the first MS studies made in thick but well-bedded platform limestones (Hladil et al. 2002; da Silva and Boulvain 2002, 2003), the importance of

these shallow-water carbonates for the stratigraphic MS records is emphasized of taking into account impurities that were widely distributed in atmosphere and ocean surface layers. Such thick series of beds, particularly if related to sufficient and continuous basement subsidence, reduced effects of major sea-level falls, river deltas or tectonically controlled shedding of clastics, may also have a good potential to provide other details on MS variations. This is simply due to the fact that there is more space for record and sampling.

Aims and possibilities

The initial motivation for the present study grew out of a perceived need for a sufficiently long composed section in which the various time-related MS variations can be precisely characterized and used for correlations. Accompanying this motivation was the real opportunity to achieve a specification of the MS curves in combination with field and laboratory gamma-ray spectrometry (GRS). The combination of four variation curves, MS and GRS with K, Th and U, was suggested as a preferable option to acquiring the appropriate proxies for the detection of ultrafine and indistinctly embedded impurities in these limestones (Hladil 2002), and it is mainly due to the fact that the direct determination of these impurities seems to be linked to serious problems. The first class of problems is closely related to the distribution of micrometric to nanometric and often complex non-carbonate particles and inclusions in pure limestones where only a part of them can effectively be separated and identified using the standard methods. And the second class of problems is related to slightly developed techniques for unambiguous classification of various generic sources of impurities. Although we are aware that a comprehensive solution of a system with complicated dynamics of mixing among impurity components is rather beyond the scope of a single study, the second motivation was to find at least the basic relationships between the GRS–MS characteristics and quantity and quality of impurities.

The section

Location and segments

The rocky landscape of the Moravian Karst and adjacent sites (Fig. 1) yields a number of sections (Hladil 2003) where well-stratified successions of *Amphipora* or other stromatoporoid-coral wackestone/packstone or packstone/grainstone beds prevail (Zukalova 1971; Hladil 1983, 1994). The appropriate parts for the composite section, however, had to be chosen according to a good preservation of rocks and strata, and a relative comparability of sedimentary features was also significant—in this case, the occurrence of flat and continuously aggraded banks with *Amphipora* horizons. This

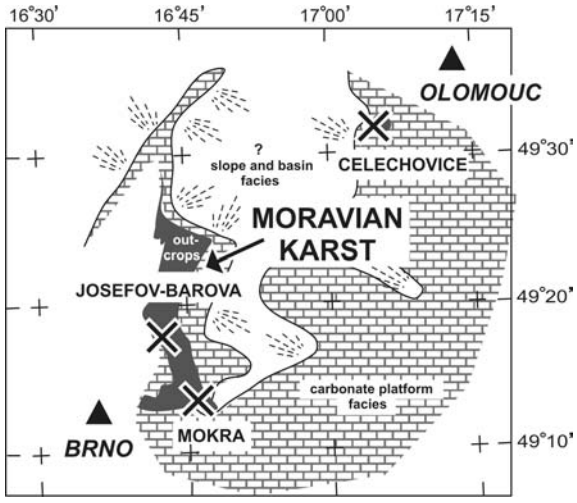

Fig. 1 Location. Three parts of the Moravian Karst Composite Section (Celechovice, Josefov-Barova and Mokra). Two auxiliary (bridging) segments of Josefov-Pila and Mokra-Western Quarry plus are immediately W of the Josefov-Barova and Mokra WQ sections. The large outcrops of Devonian platform/reefal limestones NE of Brno (*black*) are distinguished from the mostly covered parts of these limestones (regular brick-like fill pattern)

section was, therefore, finally assembled from three long sections in relatively unfaulted blocks of limestone (see Fig. 1, for location; Figs. 2, 3, for structure), where the lower (Eifelian-Givetian) part is the Celechovice Statni Q. (NE of Moravian Karst, near Olomouc—Galle and Hladil 1991; Hladil et al. 2002), the middle part (Givetian) is the Josefov-Barova Section (central Moravian Karst, N of Brno—Zukalova 1971) and the upper part (Givetian-Frasnian) is the Mokra Quarry West (SE of Brno—Gersl and Hladil 2004a). The connections of these three parts were made using the complementary sections of Josefov-Pila (lower/middle joint) and Mokra Q., fourth Level (middle/upper joint), which were selected according to their completeness and intensity of signals that were comparable to the main parts of the section. The overlapped records of signals from different sites were connected in levels, where correlation on 2 m windows in preliminary measured ends was higher than 0.8 and the values at stratigraphically corresponding points differed $< 20\%$. The end-point of the lower part was cut and replaced by the new beginning point of jointed part of the section.

Stratigraphy

The biostratigraphical scale of standard conodont zones was juxtaposed according to most recent data, as available (Eifelian—Hladil et al. 2002; Givetian—Galle et al. 1988 and Frasnian—Gersl and Hladil 2004a). This correlation has solid conodont documents in the Frasnian, and to a lesser extent Eifelian/Givetian Kacak-event levels (Hladil 1994; Hladil et al. 2002; Crick et al. 1997), but the accuracy can be reduced by coral–conodont relationships in mid-Eifelian and

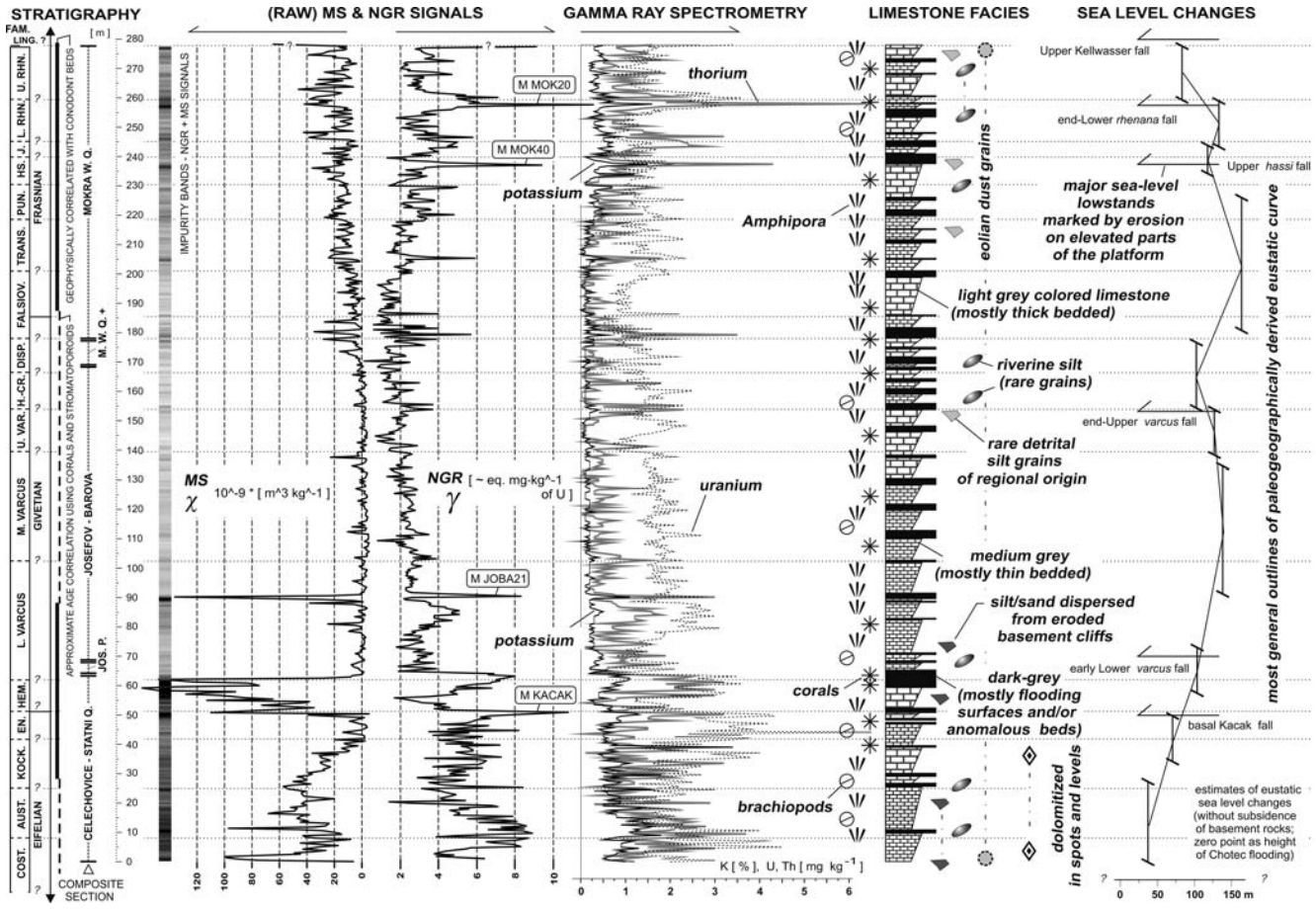

Fig. 2 The "raw" NGR (natural gamma-ray, GRS, gamma-ray spectrometry) and MS (magnetic susceptibility) values, plotted and juxtaposed with stratigraphic and facies data. The plots correspond to data for 0.5 m intervals (compare ESM1). The term "raw" means that no other recalculations were used, and scales are linear. High-impurity concentrations at the beginning (and end) of this carbonate megasequence combine the primary (input) and secondary (rate of carbonate accumulation) reasons

mid-Givetian intervals (Fig. 2). Mainly the conodont zone boundaries (correlated using the other faunas, lithology and geophysical logs far into the platform inner parts) have only approximate character. The development of various biostratigraphic tools in platform limestone facies (summarized by Hladil et al. 2002) led us to conclusions about their relatively low resolution, and this fact was one of the main arguments for us to use the GRS–MS correlation techniques. This composed section through a (mega)sequence of reef-platform limestones embraces practically all available strata from mid-Eifelian to end-Frasnian levels. The only exception is a small volume of Emsian–Eifelian limestones which have small and weathered outcrops in shear and fault zones.

Settings and environments

The effects of open ocean environment successively increased in lower part of this sequence, with an opposite trend in its uppermost part (typically in the inner, not outer parts of the platform; Hladil 2002). The conditions with continuous subsidence, slopes exposed to more than 1 km deep oceans, thickness of several hundreds of metres, and no direct contact with river deltas (Babek 1996; Bosak et al. 2002) are generally favourable for the GRS–MS stratigraphic correlation. The vertically accreted pile of carbonate banks grew on a deeply eroded and thinned block of Cadomian crystalline rocks under conditions of crustal extension (Eastern Brunnia microcontinent; Moravian structural block—Hladil 2002). The formal name of this Devonian limestone unit is Macocha Formation (Zukalova and Chlupac 1982). These limestones covered both the crystalline rocks (granitoids, gneisses, ophiolites and schists) and erosion relicts of mostly Lower Cambrian formations with sandstones, conglomerates and marine siltstones. Most recently, the thickness of Devonian sandstones was constrained to be only a few of metres (Vavrdova et al. 2003), and these sediments between the oldest beds and limestones have very local origin and are often absent, having $< 1\%$ volume if compared with the Macocha Formation. The rare lenses of sandstones in limestones correspond only to 1‰ by this comparison. These lenses are detrital rims around small crystalline, mostly granite

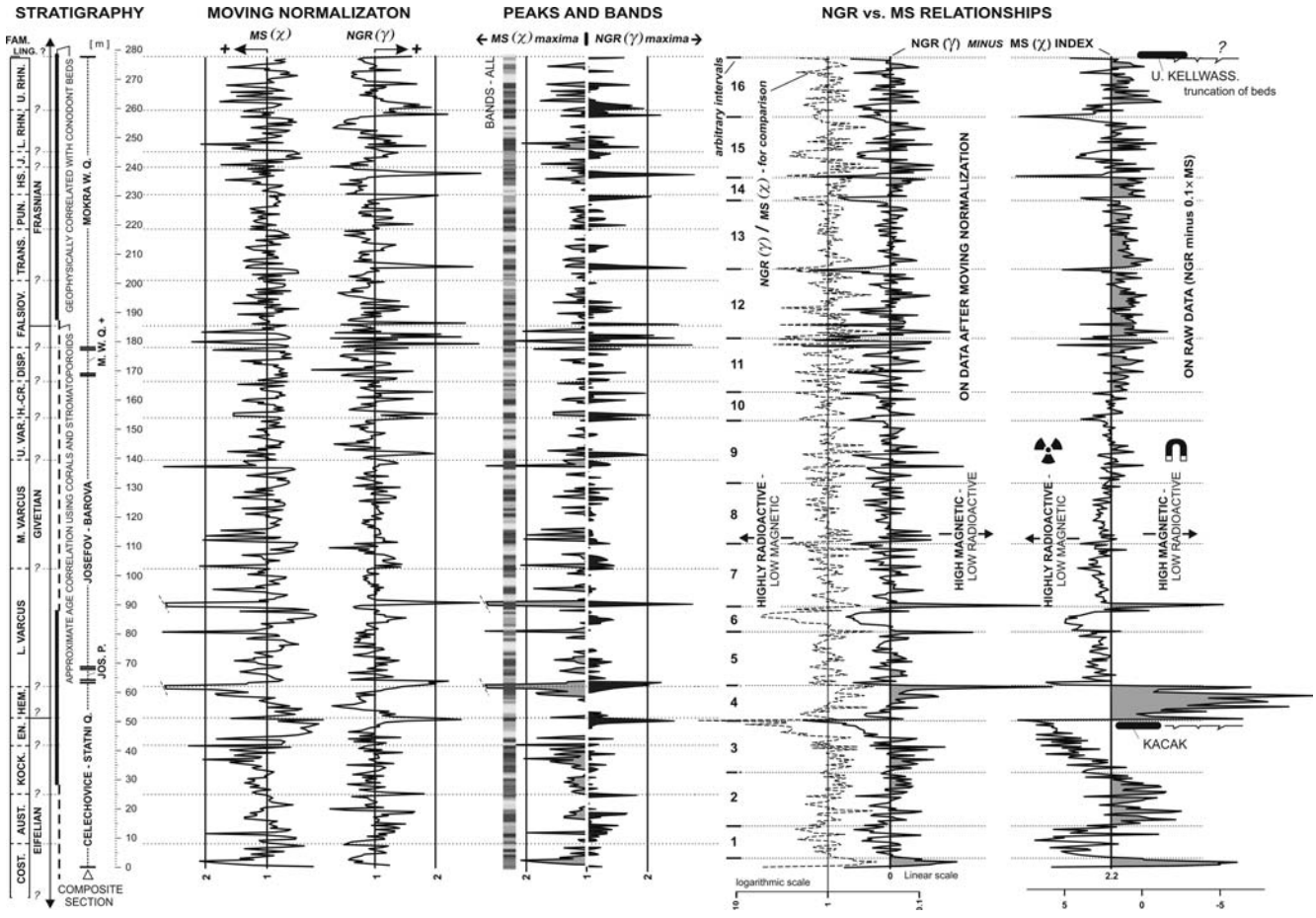

Fig. 3 Modified plots of data after "moving normalization" and comparison of NGR and MS signals. The "moving normalization" (mn) normalizes the value in each level to average value of adjacent interval (5 m window; 0.5 m shift). The comparison of MS versus NGR peak values, as well as the NGR_{mn}/MS_{mn}, $NGR_{mn}(-)MS_{mn}$, and NGR(-)MS ratio and indexes, were further used for graphic visualizations of relationships between these two sources of information on impurities in limestones. The effect of "dirty" beginning (and end) of the section was eliminated

inselbergs, which were several tens of kilometres distant (Bosak et al. 2002).

Methods

Gamma-ray spectroscopic measurements

The field measurements were made in rows of targets which were spaced 0.5 m in the section, using the GS-256 NaI(Tl) 2×2″ spectrometers in the field, and GR-320 LAB for laboratory samples. The results were directly recalculated to contents of K, U and Th. The total counts from field measurements related to "natural gamma-ray (NGR)" (> 840 keV) were converted to values of equivalent U concentrations that can produce the same effect, and thus it has only relative importance. The ~95% signal in field measurement corresponds to 0.25 m radius hemisphere (~180 kg of the rock), and several 1 kg samples were used for comparative laboratory measurements. The horizontal branches of field measurements have errors 2σ 5–15 %, which largely correspond to natural variations in amounts of bioclasts in the beds. The optimum conditions for field measurements require full perpendicular contact of the probe front to clean and flat vertical rock face, with sufficient time for stabilization of counts (we used 240 s). The complex information about GRS methods is available in a monograph by Gilmore and Hemingway (1995).

MS of the rocks

The "averaging" methods of MS logging of outcrops like with the field GRS were practically impossible, because the commercially available instruments for this purpose have small magnetic coils and much lower sensitivity than it is required for relatively pure limestones. It was substituted by detailed sampling and laboratory measurements of MS values. Approximately 40 g samples in vertical section were spaced at 5–20 cm intervals. Besides the samples in this vertical row, a horizontal sampling of single horizons was often made,

to improve, if necessary, the quality of data. These horizontal rows of MS values have not an insignificant error 2σ of 10–30%, which is twice as much as at GRS, but it can be demonstrated that these errors from natural variability of rocks do not significantly change the main patterns in the plotted curves. The values for 0.5 m points representing the section were derived from smoothed curves. Sampling of fine-grained rock matrices was generally preferred, and each sample consisted of several chips to minimize the effects of AMS. The routine measurements were made on KLY-2,3 and 3S kappabridges. The isothermal remanent magnetization (IRM) acquisition and alternating fields (AF) demagnetization was measured in direct-current field up to 0.9 T using a LDA-3A demagnetizer and JR-5A spinner magnetometer (Agico). According to terminology and methods we can refer, in general, to Dunlop and Ozdemir (1997).

Geochemical characteristics

The limestones corresponding to selected peaks, lows and patterns in the NGR and MS curves were analysed for rare earth (REE) and other trace elements. The largest number of analysed points (45 of 65) was concentrated in the Josefov-Barova section. The same finely powdered rock materials were used for all types of the analyses and small remaining amounts were saved for possible further use. The trace element analyses were made mostly using the instrumental neutron activation analysis (INAA), because it gives information about inclusions of any nature and size. Trace element analyses of carbonate samples were also performed on a quadrupole based ICP-MS (inductively plasma-mass spectrometry; VG PQ3). The samples were homogenized in an agate mortar down to 200 mesh. The powders were dissolved in $HNO_3 + H_2O_2$ and/or $HF + HClO_4$ mixture. Significant higher recovery for high-field-strength elements (HFSE) Nb, Zr and Hf were observed in $HF + HClO_4$ acid dissolution. The other analyses: C and O isotopes of carbonates, total organic carbon (TOC) and, on a few places, also extractable organic matter.

Complementary mineralogical and rock analyses

These data cover mainly the GRS and MS anomalies in the section. The largest (50–100 μm) detrital and authigenic grains are very rare. These were determined using the optical and energy-dispersive X-ray (EDX) techniques and mentioned in the previous papers (Ures et al. 1999; Hladil 2002). This former information was extended on the base 20 kg samples of anomalous rocks that were either dissolved in acetic acid or grinded and concentrated on the Wilfley table. The micrometric and nanometric crystalline impurities were identified using the secondary electron imaging and electron microprobe analysis (SEM-EMP; Cameca SX-100) both in residues after dissolution in hydrochloric acid and(or) on the surface of polished sections. The comparisons of SEM-EMP, PIXE and XRD analyses allowed to assess, although very roughly (not always identifiable), the delicate structures of mineral mixtures in goethite and mainly in very fine crystalline iron-containing aggregates of authigenic ditrioctahedral smectites with other identifiable dioctahedral clay minerals and micas.

Gamma-ray spectrometric features throughout the section and their causation

The main parts and both ends of the section are different

The NGR values are distinctly different between the broad middle parts and the lowermost and uppermost levels of this platform-limestone (mega) sequence. It is that a nearly complete Givetian succession of strata, together with significant intervals in adjacent Upper Eifelian and Lower Frasnian parts of the section, have typically decreased NGR by factor ~3 (Fig. 2). The earliest and latest phases of carbonate platform sedimentation differ not only by enhanced NGR (mainly on ^{40}K), but these ends are also marked by a moderately elevated Th/U ratio, where the Th and U concentrations are not so much different, and the former may even reach or rarely exceed the latter ones. These gamma-ray features correspond to tiny detrital grains which are more frequently found in micritic matrices of limestones (Fig. 2). It can be interpreted as a result of moderately increased detrital inputs with the beginning and end of this carbonate formation, although the overall increase of NGR for both the ends is also due to somewhat slower accumulation rate (e.g. conodont zones / thickness; Fig. 2).

GRS-detected potassium

The pure limestones in main parts of the composed section have both the absolutely and relatively lowest average concentrations of GRS-detected potassium (~0.2%). These ~0.2% of K can, if stechiometrically related, correspond to ~3.6% of illite (or ~2.1% of sericite), but there is a problem that average contents of all residues insoluble if formic acid are not higher than ~2%. This disproportion may also correspond to these findings that a significant part of the ICP-MS determined K was found even using the "soft" $HNO_3 + H_2O_2$ digestion of carbonate samples. In spite of the fact that this problem with excess of K was reported first by J. Jarka (unpublished), on the base of classical inorganic chemistry, the exact distribution of K in all non-carbonate and carbonate mineral phases has not yet been understood in details. It seems that at least a part of this excess of K is located in tiny oxidic inclusions in calcites.

It is noteworthy that the GRS-detected bulk concentrations of K are almost twice as high as those in analytical results from the point samples. The X-ray mapping and radiography of rocks suggest that this difference is caused by a strong re-concentration of impurities along solution seams. These intermittently occurring networks of waved lamellae and thin lenses typically escape the techniques of normal limestone sampling in which solid fragments of rock prevail. It seems that this disproportion between the bulk-rock and point-sample data can be found elsewhere in the limestones with common dissolution features.

Significance of relatively high uranium contents

The substantial middle parts of the section have relatively high values of uranium (averages 1.7 mg kg^{-1}). This enhancement of U values is commensurate with the Th/U and 10^4 Th/K ratios ~0.3 and ~2.9, respectively (Fig. 2). Morevover, if it is computed for the entire section, these proportions remain quite similar: Th/U ~0.5 and Th/K ~2.25. These consistently higher U than Th concentrations are rather unusual than normal for sedimentary limestones. Such concentrations are actually in inverse proportion, particularly if it is compared with limestones of epeiric seas (e.g. Lower Cretaceous of N France; Ruffell and Worden 2000) or those of ocean sea slopes (e.g. Lower Devonian of Barrandian area; Slavik et al. 2000), where the Th/U ratios are typically equal to ~2–3 (or more). Our shallow-water platform Th/U values can be seen still as inverse also if pelagic cherty limestones of the world ocean are compared (Plank and Langmuir 1998). These examples from distant and deep ocean environments suggest that a single parameter of distance from direct detrital sources is not the most significant condition for occurrence of such low Th/U values.

Hence, the very low Th/U values are quite rare in sedimentary carbonates. One exception of this rule, with values about 0.3–0.5, was found in an Upper Cretaceous marly-cherty euxinic system of the Venezuelan La Luna Formation (Lo Monaco et al. 2002). Of course, this is a very rare example that is almost unrelated to Moravian Karst, because the TOC and vanadium concentrations in these oil rocks are more than ×25 and ×2,000 higher than here (reaching ~5 and 0.4%, respectively). Looking for certain Devonian counterparts with dysoxic deposition of limestones, we can mention the goniatite beds of Kostomloty (Kielce area, Poland). In spite of occurrence of framboidal pyrite and 1%-TOC content, their average Th/U values oscillate about ~2 (Bond and Zaton 2003; Racki et al. 2004). Similarly the carbonatic black shales and limestones of Lower Frasnian age in Algeria kept the Th concentrations higher than U still at 14%-levels of TOC (Luening et al. 2004). Thus, the low Th/U ratio in limestones of the Moravian Karst can hardly be explained using the possible effects of euxinic waters and high TOC contents. As a direct evidence for this, we can mention the low average concentrations of TOC (~0.2%) and low correlation between U and TOC (~0.4) which is only slightly higher than for Th and TOC (~0.3).

However, a more plausible comparison we can make is with the GRS measurements in vertical sections throughout the young carbonate beds of the NE margin of the Great Bahama Bank (e.g. Hladil et al. 2003b). Here, this predominance of U over Th (= low Th/U ratio) is an undoubted feature of limestones, and it is clearly related to extremely shallow-water but oceanic character of deposition which is combined with embedding of impurities from settled African dust (and impurities recycled on place). These impurities in carbonates of Recent Bahamas are typically rich in Fe but are a little depleted in K (see the "Other geochemical characteristic" for explanation of this difference). A substantial, although not absolute, similarity of the Bahamian impurities and their GRS images with those of the Moravian Karst (Hladil et al. 2003b) allows us to give an approximate idea of what the inputs, making the impurities of this sort, actually are. A significant role in the formation of these impurities is likely for atmospheric desert dust transported over long distances.

Sea-level falls, impact-related horizons and primary banding of impurities

These remarkably low Th/U values of the Moravian Karst section are, however, disturbed occasionally by narrow and sharp anomalies where the values for this ratio are increased, reaching the values about 1. These anomalies often correspond to major eustatic sea-level drops, e.g. with the end-Upper *varcus* or Upper *hassi* falls (Fig. 2), but they are also linked to possible meteoritic impact horizons (Hladil et al. 2004), e.g. with the stratigraphic markers of Kacak, Josefov-Barova-21 or Frasnian *punctata* horizons (Fig. 2). All these perturbations have paleogeographic significances in themselves that correspond to (1) emergence of local crystalline inselbergs and spreading of detrital grains from this source, (2) increased eolian flux of mineral dust from other substantially emerged landmasses and continents elsewhere and (3), but only in humid climates, the development of river networks that provided increased quantity fluvial particles (Hladil 2002). The latter type of input is particularly relevant to first flooding surfaces—e.g. Celechovice (Ures et al. 1999; Hladil et al. 2002). Here, also Fe-glauconites together with slightly increased phosphate were found, and this is likely to be typical of rather sediment-starving carbonate systems where eolian and riverine inputs were mixed together.

According to comparison with paleogeographically derived eustatic curve and structure of flooding surfaces in the limestone facies column (Fig. 2), it can be postulated that GRS fluctuations in these limestones are

basically recording the eustatic changes (Gersl and Hladil 2004a; b). However, a large number of secondary differences from overall facies changes had to originate mainly due to certain dissonance between local and major interregional rhythms of sea-level fluctuation as well as from very incompletely known ocean and atmospheric circulation that was directly responsible for an unstable, rather punctuated delivery of detrital and eolian material on the platform.

Hence the increased concentrations of complex impurities of varying compositions form narrow and sharp anomalies in the section (Figs. 2, 3), and this feature is not merely relevant to partial low-stand sedimentary condensations but equally to these increases in episodic delivery of non-carbonate material. The evidence for this is that laboratory GRS, X-ray maps and radiography suggest that such a banding, where obscure impurity bands are often arranged with large spaces in between, exists also in scales of centimetres and decimetres. This fine-impurity banding matches only in 40–60% the most obvious changes related to bedding and material of the beds how these are perceived in the field, and it also has a practical impact on relationships among the GRS, MS, beds and facies in detail, as substantiated also by partial segments of the section (Fig. 4, for example). Consequently, the direct relationships between the arrangement of beds and facies of these platform limestones and their GRS records would not be overestimated.

MS variations and their possible carriers

Overall characteristics of magnetic mineral phases

Magnetic susceptibility in limestones with impurities is generally considered to be a physical quantity that can be used for the indication of concentrations of iron, ferromagnesian or clay minerals. It was documented that this MS signature in various marine limestones substantially resides in paramagnetic detrital or detrital/authigenic constituents of the host carbonate rocks (e.g. Ellwood et al. 2000). Of all the paramagnetic minerals in limestones usually the most abundant are smectite–illite, chlorite and micas; chloritoids, glauconite and siderite, if these minerals are present, have stronger MS effect than modest amounts of disseminated pyrite.

However, the XRD analyses of insoluble residues from the Moravian Karst section found regularly the predominance of smectite–illite, micas (sericite, with quartz) which occur in the ambient carbonate matrices together with goethite. Other minerals of significance in MS of limestones are pyrrhotite, pyrite, hematite, ilmenite, magnetite, other combinations of Fe-oxides, often with Ti, and pyroxenes, but their amounts and crystal sizes are usually very small so that it is difficult to physically separate these minerals from the embedding mixed mineral matrices. The INAA-determined average

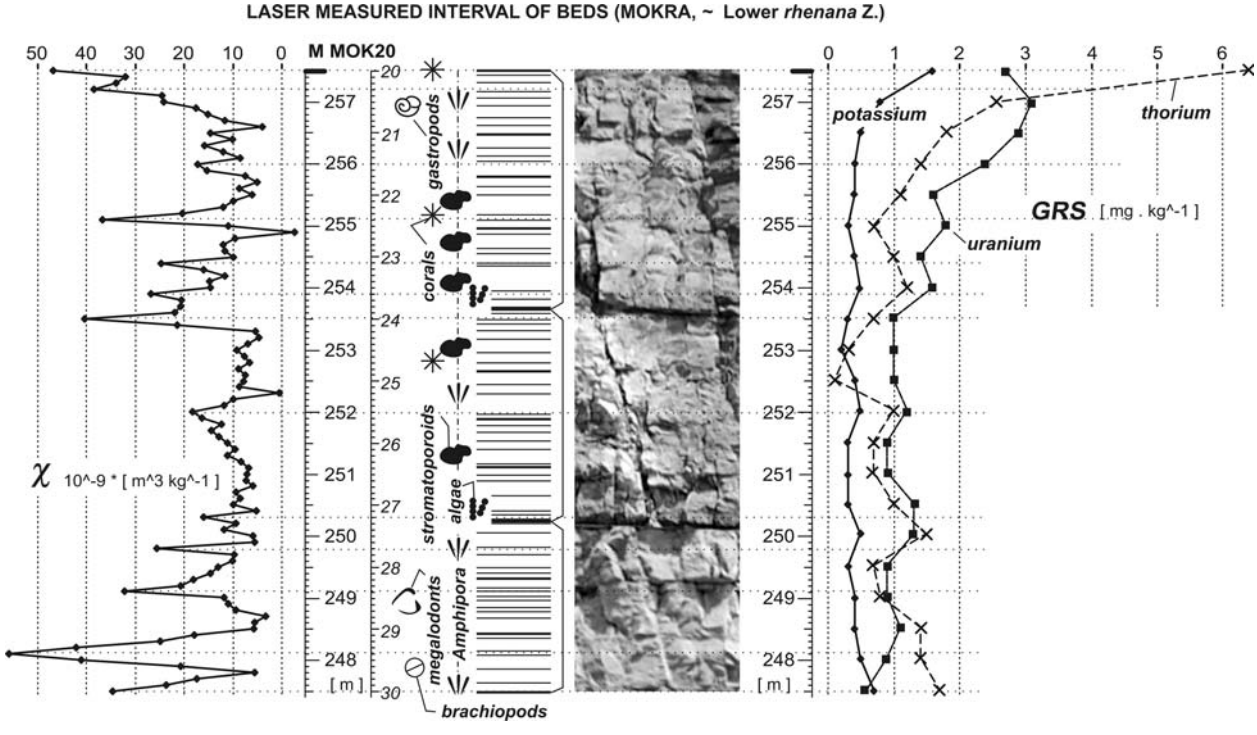

Fig. 4 A detailed window from the Lower *rhenana* interval of beds. This, and also any other details of the section yield evidence of limited consistency between GRS–MS and lithology–biofacies data. The variations of these parameters are much more independent than usually portrayed. Examples of strong anomalies inside the massive beds (248.1 m) and, inversely, the minima at contacts of the beds (256.5 m), occurring irregularly, are corroborating documents to primary eolian input of impurities in these limestones

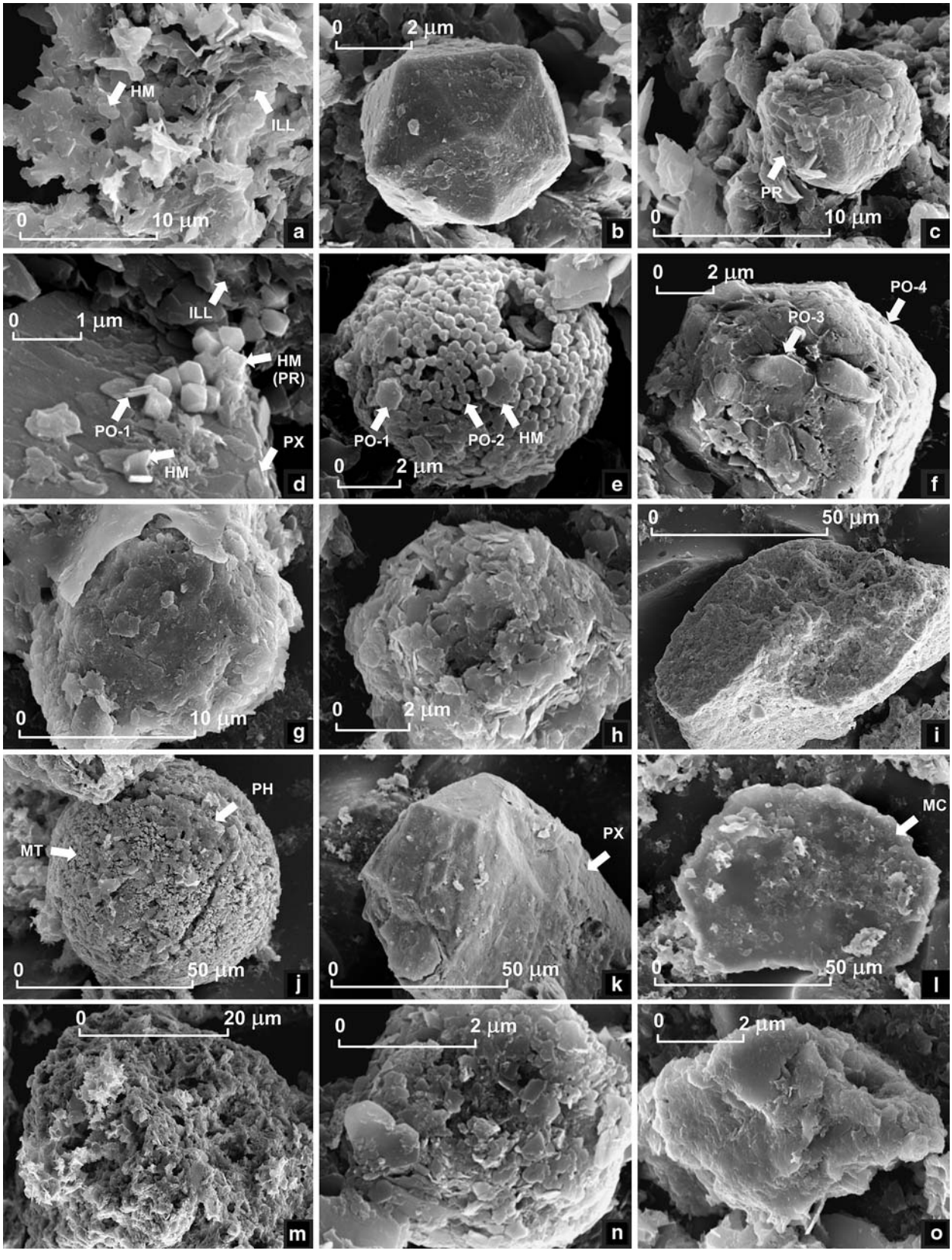

content of Fe in these limestones is 0.1 wt%, and about 70% of this iron is, in average, extractable using the soft dissolution in $HNO_3 + H_2O_2$ (ICP-MS). It suggests that iron is mostly bound in oxide and other possible easy dissoluble phases (Fig. 5 a, d, e, g, i, for example), and only lesser amounts are tightly bound in sulphide and

◄

Fig. 5 Scanning electron micrographs. The images document a selection of singular particles and crystals which were found individually in the relatively uniform and very fine structured, originally very fine particulate smectite/illite/sericite–goethite/hematite groundmass of complex impurities. Samples: 90 m, Josefov-Barova-21 (images a–f); 238 m, Mokra-40 (g–i); 258 m, Mokra-20 (j–o). **a** Assembled clasts and crystals of illite/mica compositions, with dioctohedral structures (ILL); accessoric minerals are embedded as submicrometric rounded polyhedra and rods; scales of hematite are present (HE). **b** Spectacular icosahedral crystals (max. 5–6 μm) are rich in Zr, Si with modest contents of transition metals, with actinoids. A few crystals like this one. Icosahedron (regular 20-faced polyhedron) is an extremely rare shape, which is almost unknown among minerals occurring in nature and seems to be linked rather to artificial HP-HT minerals. **c** A cube of late diagenetical pyrite (PR) is coated by phyllosilicates and hematites and has, on its upper and left sides, imprints of carbonate crystals. **d** Submicrometric hematite pseudomorphs after pyrite, HM(PR), with negligible content of sulphur, along the contact between a small crystal of pyroxene composition (PX) and coarse mica/illite aggregates (ILL). Bent scales of hematite (HM) and subhexagonal platelets of pyrrhotite composition (PO-1). **e** The spherical layer consists of 250 nm pyrrhotite (PO-2) pseudomorphs after pyrite, but the interior of such spheres is usually filled by carbonates, illite/mica and hematite. The upper surface is covered with adhering scales of hematite and pyrrhotite (PO-1). This shell-like shape resembles rather a relict of a sphere (like pyritized coccospheres today) than framboidal pyrite. **f** Prismatic rods of sulphur-deficient pyrrhotite compositions (PO-3) inside a hexagonal platelet of pyrrhotite (PO-4). **g** Relatively pure, compact illite/sericite micronodules, which are coated by problematic amorphous mineral films rich in organic matter. **h** A mica/illite bead of less compact structure. **i** A large, rounded clast (very fine structure, mostly with sericite and iron oxides); a grain indicative of sediment recycling. **j** A microspherule with two major mineral types: magnetite-like-shaped nanometric crystals of iron oxide (MT) and silicates of olivine- and phlogopite-like compositions (PH). Possible meteorite material (carbonaceous chondrite?). **k** A large crystal of Mg, Fe, Si composition. An example of unweathered, rare (exotic) crystals that resemble enstatite–ferrosilite pyroxenes (PX). Source unknown. **l** The largest specimen of detrital muscovite mica. It is relatively uncommon to find them deeply inside the carbonate sequence of this type. **m** Friable material of a pellet—a spongiform complex residue with typical illite outgrowths and many hollows after dissolved carbonate crystals. **n** A small mica/illite pellet with adhering hexagonal platelets of dickite-kaolinite (Al-rich) compositions. **o** A dense aggregate of mica-clay minerals of remarkably variable proportions of major elements (K, Al, Mg and Si); traces of cobalt

silicate minerals (Fig. 5 c, d–f, j and k). It contradicts the predominantly paramagnetic origin of the MS and suggests that composition of Fe-rich impurities is not so much based on the detrital clay minerals as can be assumed, for example, from the comparison with impurities in the Givetian-Frasnian platform limestones of Ardennes (Chamley et al. 1997; da Silva and Boulvain 2005 in press).

Extent of MS variation

In the Moravian Karst section, the highest MS values of $\sim 160 \times 10^{-9}$ m^3 kg^{-1} in 0.5 m-interval data (and $\sim 350 \times 10^{-9}$ for 5 mm thin anomalous laminae) correspond to the maximum concentrations of Fe which are 0.7 wt% (and 1.6 wt%, respectively). Broadly, the mass MS values in this section range between several tens, in rare anomalous layers also more than a hundred of 10^{-9} m^3 kg^{-1}, and slightly negative values of the purest limestone intervals (Fig. 2), where it is caused by diamagnetic properties of calcite. The most pronounced MS anomalies in the section were found at the Kacak Event and in a zone close above, and the other corresponds to the Josefov-Barova-21 stratigraphical marker (Figs. 2, 3). These elevated, sharp "spikes" in MS plots likely correspond to bolide events (e.g. Ellwood et al. 2003, for the Kacak E.), and high MS is ascribed to the occurrence of ferrimagnetic minerals, primarily magnetite/maghemite and pyrrhotite. However, an increase of MS values over a relatively broad interval at ~25 m below the Kacak E. is different, being rather compared with occurrences of hematites (Fig. 6e, f), and a strong enhancement at ~10 m above this event horizon has been explained by the occurrence of numerous ferric inclusions in honey-coloured Fe-glauconites (Ures et al. 1999).

MS as an indicator of average concentrations of iron

The correlation between MS and INAA- or ICP-MS-determined concentrations of Fe, based on 45 points from the Josefov-Barova interval of the section, is very high, exceeding 0.9. A slightly decreased correlation values between these two quantities characterize the Mokra and Celechovice beds in the section, ~0.8 and ~0.7, respectively. It gives direct evidence about the reliable MS detection of total Fe in these Devonian platform limestones and puts constraints to the observed mineralogical variations of clearly visible tiny crystals of Fe-oxides and sulphides in residues which seem to have far less effect than might be expected. It can be related to several conditions, e.g. limited amount of well-crystallized specimens, the presence of impure mineral phases and the diversity of coexisting varieties, where the latter can be enhanced still further by weathering of these minerals (SEM-EMP: structurally and chemically altered tiny grains of magnetite, pyrrhotite or ilmenite).

Constraints to effects of organic matter on the occurrence of magnetites

Considerable weak relationships were found between the variations of MS and TOC concentrations. The MS–TOC correlation value for the middle part of the section (Fig. 7) is low ~0.35, slightly higher for the lowermost but very low for the uppermost part. The direct correlations between TOC and INAA- and ICP-MS-detected Fe concentrations are similarly low, but there are slightly higher values for difficultly than easily extractable Fe (~0.32 vs. ~0.21). This may tentatively be explained in terms of a poor HNO_3-solubility of

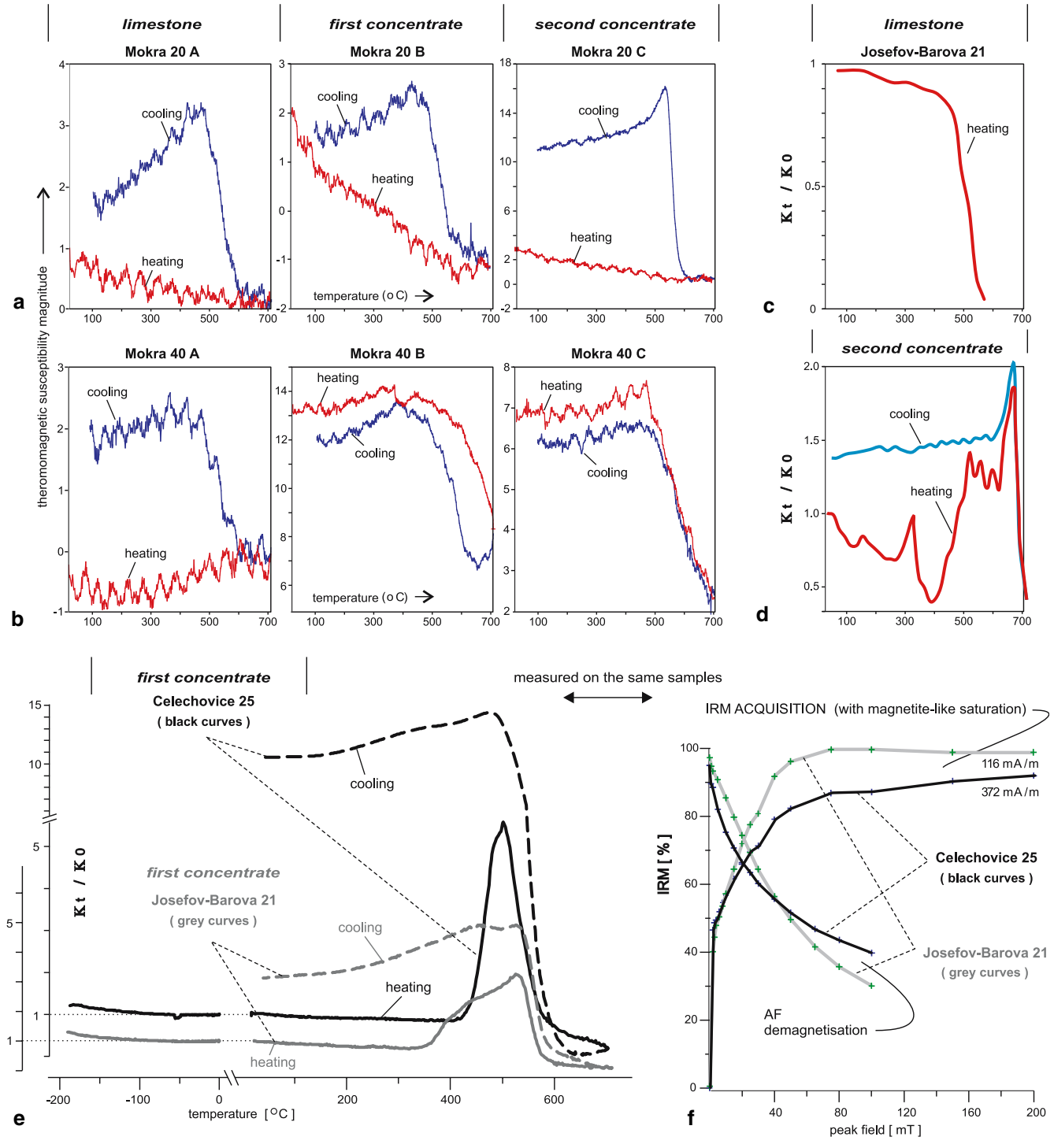

pyrrhotite, which can directly originate in sediments (e.g. ~0.2–0.5% of TOC, low total-S and high concentrations of easy extractable Fe; Kao et al. 2004) and may also be formed at both the natural and experimental heating of greigite that can be considered as a possible precursor (greigite → pyrrhotite + magnetite; Lennie et al. 1997). Small concentrations of pyrrhotite in this section were found mainly using the SEM-EMP (Fig. 5 d–f).

The exact documentation of small amounts of magnetite in these rocks is far more complicated than for pyrrhotite, although the limestone samples in the interval around the relatively highest MS values in the lower (Josefov) part of the section provided the typical shapes of demagnetization curves for magnetite (Fig. 6c; Krs et al. 2001). However, the MS–TOC correlation is slight also if detailed variations are investigated in this interval of strata. The sources of

◀

Fig. 6 Thermomagnetic behaviour of imperfectly separable mineral mixtures. Several contrasting curves relate to four anomalous horizons (Celechovice−25 at the 25 m mark, Josefov-Barova-21 at 90 m, Mokra-40 at 238 m and Mokra-20 at 258 m, in metres of the composed section). There types of material were used: original limestones and the first and second concentrates of their impurities. The first are gravitational (Wilfley table), and the latter were obtained by dissoluting them in 20% CH_3COOH (HCl for Josefov-Barova). **a** Samples from the uppermost part of the Lower *rhenana* interval. A complex record of phase changes: e.g. the 20-B image has no evidence of accessory hemoilmenite (found by SEM-EMP), but it slightly indicates the presence and/or formation (and decay) of low-temperature maghemite or Ti-maghemite (F. Hrouda, personal communication). The shape of the these heating curves can also be affected by thermal decomposition of pyrite to pyrrhotite in mineral mixtures (J. Hl.), and a paramagnetic signature is likely involved in the initial MS of all the Mokra-20 samples (B.B. Ellwood, personal communication). However, the main XRD-detected components are calcite, quartz, illite/micas, with traces of pyrite/pyrrhotite at 20°C, and the features of the latter are absent after the heating to 700°C, so that proportions of all other, albeit diversified, accessory minerals in these complex impurities are limited to a few tens or first %). **b** Other Frasnian stratigraphic marker; Upper *hassi* interval. Calcite, quartz, illite/micas prevail in 40-B, but phyllosilicates with Fe and Fe-oxides are in admixtures. A very slow MS decrease at Curie temperatures may correspond to inhomogeneous zonal titanomagnetites (F. Hrouda, personal communication). In general, the ferrimagnetic effects can be found in all Mokra-40 samples (B.B. Ellwood, personal communication). (A and B: measurements by B.B. Ellwood). **c** The black coloured raw limestones of the JOBA-21 mid-Lower *varcus* event horizon often show the heating curves which are indicative of accessory magnetites, although the values drop early, at 510°C (the heating curve, by M. Krs in 1992). **d** The decarbonatized dense concentrates related to the above-mentioned event contain pyrrhotite; they have typically blackish colour in solid state, producing dark-grey greenish solutions in HCl. The susceptibility versus temperature curve (extremely low rate of heating/cooling, in air; in KLY-2 Suchdol) is indicative of pyrrhotite/pyrite phase changes at low temperatures, but the changes at higher temperatures may correspond to structural assembling of magnetites and hematites. Anomalous features are two: an apparent valley in heating curve at ∼400°C and very late Hopkinson peaks, e.g. at ∼650°C. **e** Faster (2 h) thermomagnetic treating of similar but relatively less concentrated residues, in KLY-4 s Pruhonice; Josefov-Barova-21 and Celechovice-25 are compared. The relatively smoother shapes show one high peak on the Jos–Bar gravitational concentrate which is centred at ∼525°C, and other, in the Celech. sample, at ∼500°C. The values in cooling curves are apparently higher than those in the heating trajectories. **f** The magnetic behaviours of these residues with IRM acquisition and subsequent AF demagnetization. It suggests that the behaviour of the Jos–Bar first concentrate can be related to magnetites, whilst the Celech. concentrate is indicative of greater concentrations of hematites

problems are dual. For the first class of problems, there are various SEM-EMP indications that these magnetites are likely late diagenetic, as they can occur as pseudomorphs after sulphides or forming spotty and altered inclusions in smectite–clay–mica impurities. And the second class of problems relates to very small amounts of this mineral, nanometric sizes of specimens and their coalescence with other oxidic and sulphidic phases of Fe. There is still no convincing evidence proving that the primary bacterial magnetites are really preserved in these rocks, although it cannot be completely excluded (Hladil et al. 2003b). Using the published data on magnetites and their effects in marine sedimentary rocks (∼1.75 mg kg^{-1} of PSD magnetite in rock for MS of ∼$1{\cdot}10^{-9}$ m^3 kg^{-1}; Collinson 1983; Richter et al. 1997), we can surmise that the possible amounts of magnetite must generally be extremely low for these Fe-rich limestones which show only low values of MS.

These minimum amounts of magnetite are almost invisible in many thermomagnetic MS curves because of much higher contents of other minerals with Fe and intense formation of new mineral phases (Fig. 6). The possible thermal maturation of imperfect primary magnetites, if exists, is strongly overprinted by breakdown of paramagnetic phases into magnetite during the heating. An interesting feature is the often high level of cooling curve with moderate and smooth decrease towards the low temperatures. Both this very high position and decrease with cooling, on these very fine mineral mixtures, remain unexplained for now.

Pedogenic Fe-minerals and some but limited mobility of iron

The sample related to stratigraphic marker Mokra20 (Figs. 2, 3) has SEM-EMP indicated tiny grains of hemoilmenite which contains 5 μm thick relicts of ilmenite in laminae (∼36.8% Ti, 31.6% Fe). These grains were embedded in porous carbonate–quartz–illite (mica) networks with small contents of goethite and hematite. However, the content of ilmenite is so small that its MS thermomagnetic behaviour is completely overprinted by the complex behaviour of surrounding mineral mixtures (Fig. 6a). This rare finding resembles occurrences of authigenic tropical soil ilmenites that usually developed on ophiolites and basalts (Goulart et al. 1994; Doriguetto et al. 1998). The limestones on this place of the section have possible relicts of a paleosol, but this surface was truncated, and the hardground was subsequently covered by stromatolite-like structures. The authigenic ilmenite can tentatively be considered as a product of in-situ weathering, but its atmospheric or aquatic transport is also possible (compare the assemblage of objects in insoluble residues; Figs. 5j–o). The MS behaviour of Mokra40 residues with temperature is different, both the heating and cooling curves have quite similar trajectories (Fig. 6b). The residues relevant to this behaviour have a strong predominance XRD-detected carbonate–quartz–illite networks, with a number of the micrometric illite–mica beads that consist of both the smallest clasts and authigenic crystals (Fig. 5g–i).

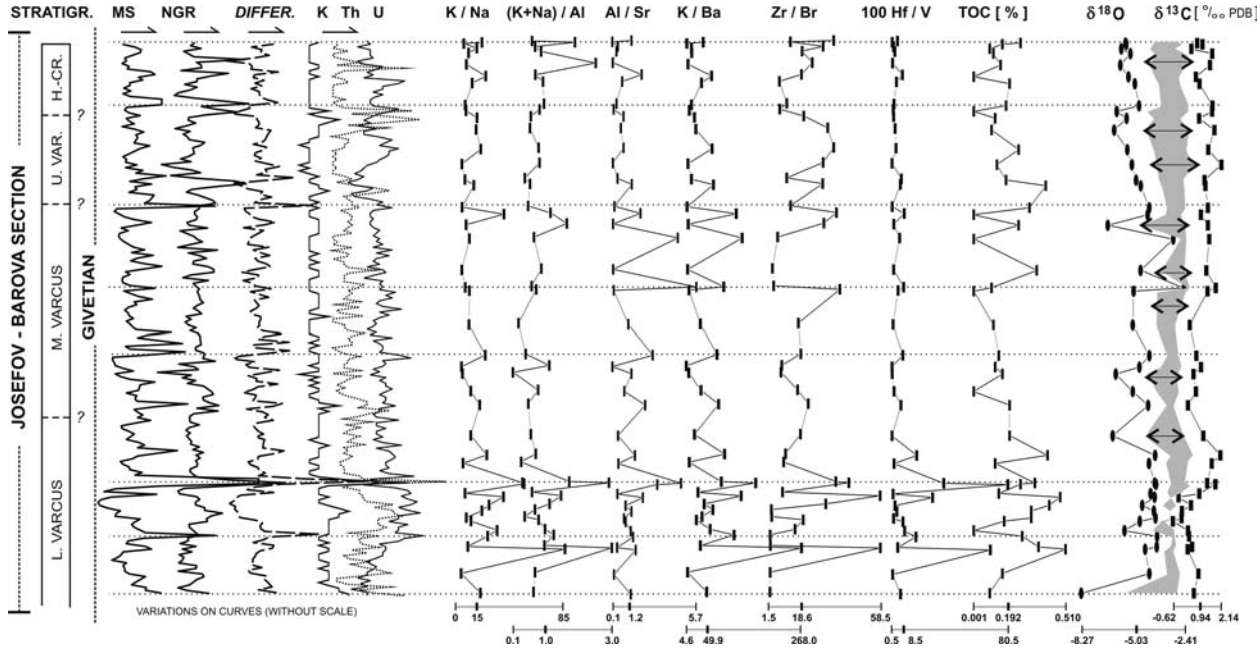

Fig. 7 Gamma-ray and magnetic susceptibility fluctuations compared with element ratios, total content of organic carbon and excursions of C and O isotopes. Large segment from the middle part of the section. K/Na and (K + Na)/Al have comparable shapes and the excess potassium is occurring often (but not always) with and before the major NGR and MS anomalies. It makes impossible explanations based on riverine particulates, which are relatively rich in Na, but opens also other problems related to this K excess (see the text). The ratios of selected lithophile elements (Al, K, Zr, Hf) to those which are more independently behaving (Sr, Ba, Br, V) are indicative for any particulate inputs. However, the similarity among these and other ratios drops dramatically in the very pure carbonates above the Josefov-Barova-21 anomaly (upper part of Lower *varcus* Z.). Most of the TOC variations are not driven by changes in impurity concentrations and, below the above-mentioned anomaly, the highest TOC concentrations were found in the purest limestone intervals of beds. And finally, the widenings and narrowings between the C and O isotope variations correspond rather to platform carbonate cycles than to different amounts of impurities in limestones—compare the GRS (K, Th), on the left

The diagenetic mobility of iron concentrations and related changes in the structure of the stratigraphic MS values can be seen along with major sedimentary cycle boundaries, where leaching and the formation of cementation zones affected the structure of primary banding by impurities (Hladil et al. 2003b). These superimposed diagenetic features related to major sea-level falls are, however, not very common in this GRS–MS section. It is much more typical for the shallowest and slowly subsiding parts of the platforms. Conversely, the processes of fast cementation, further decrease of porosity with burial and chemical/isotope evolution in closed systems (Hladil and Hladikova 2003) were rather favourable for the preservation of Fe concentrations "in situ", as they were originally embedded in these limestones.

At last, it must be mentioned that these very fine and complex impurities that are directly inducing the stratigraphic MS variations in relatively pure varieties of these limestones show a remarkably high correlation between Fe and REE or several other lithophile elements (Fig. 7, and principally 8). Because of the fact that such results in matrices of correlation values for chemical elements were never found in sets of analyses from the directly underlying or sporadically intercalated detrital sediments, we can legitimately speculate about the possibility of additional, more distant, somewhat averaged inputs of impurities that were quite stable for millions of years and might, at least partly, correspond to admixture of atmospherical particulate matter.

Comparison of magnetic susceptibility and natural gamma-ray signals

Basic similarities and particular differences

The overall correlation coefficient between the NGR and MS variations in this section is 0.48 (compare the 0.5 m raw data; ESM1). The highest correlation exists in the broad middle part of the section (Figs. 2, 3, 7) where several thick intervals yield correlation coefficients that are close to ~0.7. The correlation coefficients in upper Mokra parts of the section are the same as the average, but the lowermost Celechovice part has much lower coefficients which drop to zero or even slightly negative correlation values. And we can infer from this that the correlation is smaller than average mainly on these places where signatures of various detrital inputs were found. In general, the positive to very good correlations prevail, although the positions of NGR versus MS peaks in individual nodes of anomalous values can be shifted up and down, and

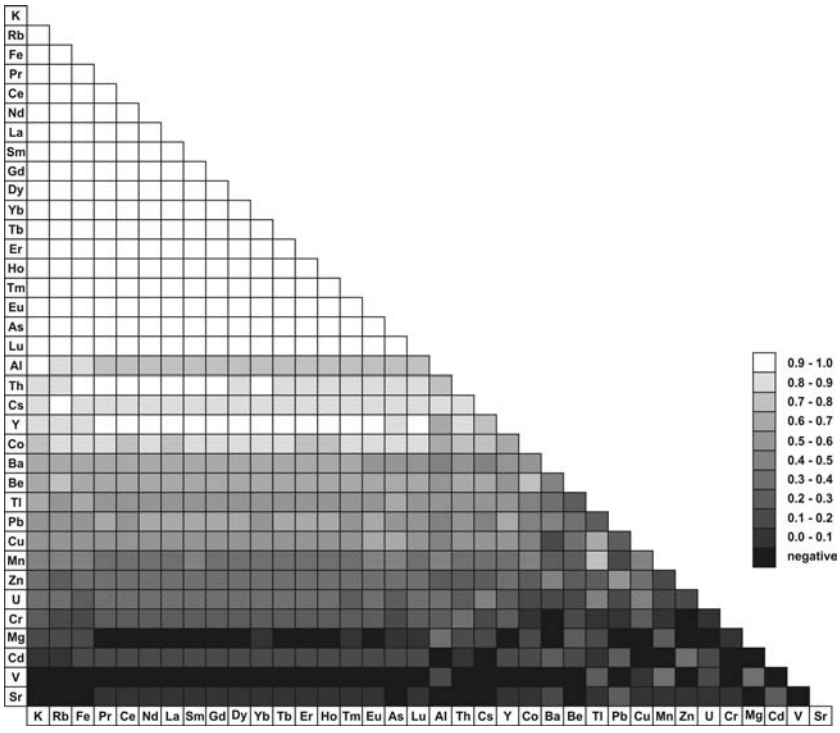

Fig. 8 A correlation matrix of selected elements that were consistently determined in 45 samples from the broad middle part of the section (INAA and ICP-MS). The absolutely highest correlation values link K to Fe and Rb, with very high correlation between them and all REE. Remarkable is strong 0.95 correlation between Fe and As, by Fe/As ratio ~800. Still high-correlation values link Fe to five lithophile elements Th, Cs, Y, Co and Al. It differs from the data about closely underlying and rarely intercalated clastic sediments with abundant goethite where correlations for Fe and REE are slight and Fe and As do not correlate at all (Fe/As ~2000). The low-correlation values for elements in the lower part of the ordered matrix reflect their complex pathways during delivery, precipitation and diagenesis

they often have different shapes and amplitudes (Figs. 3, 4). Particularly the mutual relationships among MS and three GRS quantities for K, U and Th (Figs. 2, 4) are so diversified that it can be given for studies on many primary and/or secondary influences that are still poorly understood (perhaps with a small exception for trifurcate pattern at cycle boundaries; Hladil et al. 2003b).

The nature of this variation can be seen mainly in syn- or post-depositional mobility of U and in much lesser extent, but still visibly, for Th (see Fig. 8 for correlation between these elements and Fe or K). In this context, it must be mentioned that about 85% of ICP-MS-detected U (and even more for Th) can be released by nitric acid dissolution so that only minor amounts of U and Th were stored there in $HF + HClO_4$-digested "compact" detrital phases. The above-mentioned trifurcate patterns consist in partial preservation of complex impurities at the original level, an increase in uranium and diagenetical biomagnetite in a cementation zone below, and a specific increase of U (and potentially also K with paramagnetic micas, if recycled) at a flooding surface above the cycle boundary. But exactly this type of strong early diagenetic modifications contributes to GRS–MS patterns in this section only with a few per cent, not more, and there are hundreds of details that cannot be explained so easily (Fig. 3). We shall also consider the changes in primary compositions and provenance, alterations during the transport, processes in the time span from the settling to embedding as well as other than the most ubiquitous forms of diagenetic alterations. Anyway, this variation does not necessarily be the case of chaos. Rather the opposite can be true, and this combined record may reflect a complex of surrounding conditions far better than any other methods. Of course, the best evidence of this contention will be to compare the other GRS–MS platform sections, when will be available.

High magnetic versus highly radioactive impurities

One approach that how to describe this sort of variation is the use of NGR/MS ratio, i.e. differentiating between the high magnetic but low radioactive (HM–LR) and opposite (HR–LM) features of complex impurities in limestones. According to detailed analyses of impurity banding, the HM-LR impurities have the best correlation with concentrations K, Hf, Lu, and also Fe (coefficients about 0.5 and higher) and practically the same can be demonstrated on large group of the lithophile elements. Further, TOC, Ca (or opposite, the total impurity content) and Br have nearly zero correlations so that occurrences of very pure (light-coloured) or blackish limestones seem nearly unimportant, and thus the high K, Fe dominance (and from the middle part of the section also Al) may be, in these limestones, indicative of the inputs that have no direct relationships to carbonate facies, seawater or pore water processes. A substantial upper part of the section documents a tendency to be turned towards the HM–LR side. However, the lower part of the section shows visible HR–LM trends (Fig. 3).

There actually exists a parameter which has a capability to explain this very easy. And it is a slowly

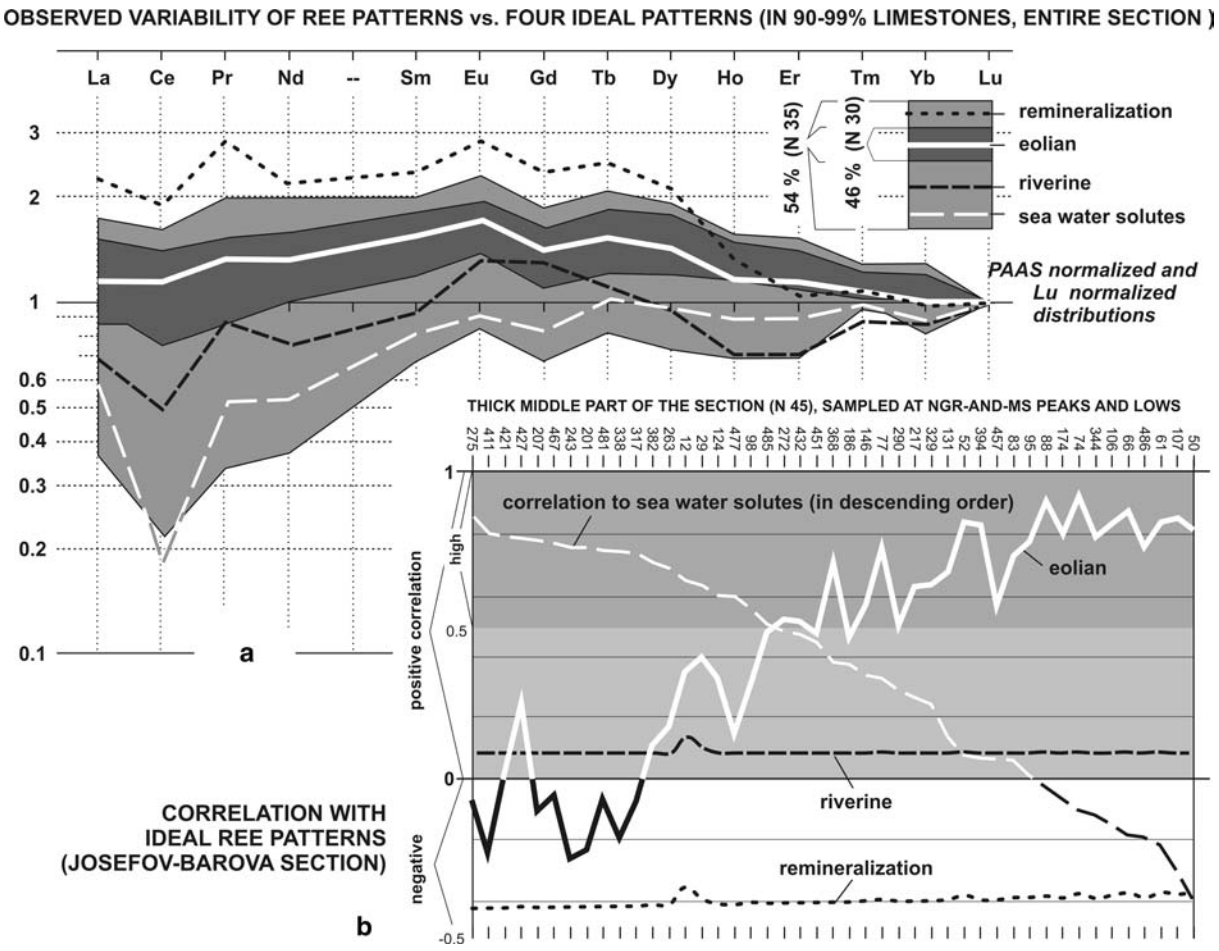

Fig. 9 The REE signatures of typical impurity fluxes in comparison with the data from the analysed carbonate sequence (see the text). **a** The majority of samples contain distributions which are practically identical to those of the typical eolian input, i.e. close to numerical value 1 in the normalized concentration values. **b** Correlation of each sample with four possible input signatures, ordered according to signature for seawater solutes. The clearly eolian signatures correspond mostly to positive MS anomalies, being exactly inverted to those of solutes. And the dominant imprint of solutes, in accordance with expectation for this system, is generally associated with the low-value intervals in MS curves which have strong predominance of calcite

decreasing content of stable heavy mineral grains throughout the section (micrometric/nanometric zircons or monazites), as it is given by successive attenuation of all proximal detrital inputs. The decrease of zircon content with increased distance of a dust plume from its source is generally known, because the long-travelled dust plumes are severely depleted in zircon due to gravitational sorting (Marx et al. 2005, in press). There are also other factors that affect this: for example, hematites (Fig. 6e) from shallow-water bacterial mats support the anomalous HM–LR shape between 15 and 30 m in Celechovice, and the occurrences of magnetites in blackish coloured Kacak and JOBA-21 m event-related beds elucidate the strong HM features in these parts of the section (Fig. 2). With the event-type spikes in MS curves, we must consider also the gain of magnetites precipitated from impact ejecta plumes, but the magnetites close to above are likely detrital and diagenetic (see MS variations, above).

Other geochemical and isotope characteristics related to fluxes of impurity precursors

Signatures of rare earth elements

In spite of the fact that a number of analysed limestone samples have a strong and quite constant relationship between the concentrations of Fe and REE (Fig. 8), there are slight differences between particular REE distributions. The different shapes and inclinations of normalized curves are mainly due to various depletion of LREE, mainly on Ce. Very approximately this depletion is relevant to time period and intensity of interaction of fine particular matter with ambient aqueous environments (Fig. 9; Nozaki 2001). The samples for REE were taken at the mid-section NGR–MS peak and low points (N 45), and other analyses (N 20) are from the upper and lower parts of the section. The basis of data which gives reasons for comparison was completed by Nozaki

(2001) who summarized the information about mean recent REE fluxes to the ocean, giving also the outlines to average remineralization, atmospheric, riverine and seawater (solutes) impurity precursors. It is significant that the atmospheric dust compositions are not very different from that of the Post-Archean Average Shale (PAAS), whereas the riverine clay input from distal sources has been moderately depleted in LREE (from La to Sm), and this depletion is even more enhanced for sea-water solutes. Thus, the left side of a normalized curve is more and more inclined and distant from the PAAS-normalized horizontal. The overall remineralization trend has just opposite effect that materials are often enriched in LREE and the left ended part of the relevant curve pitches a little upwards (Fig. 9a). The occurrence of phosphates may, for example, push up the middle part of the curve.

Because of the fact that all the complex redistributions and fractionations during the processes of embedding of very fine impurities into carbonate are assessable only in rough terms, if ever, we took as a base the real distribution field of REE as obtained according to our analyses. As a next step we fitted the above-mentioned quartet of templates (remineralization, atmospheric, riverine and seawater) into this field. An average difference between the possible impurity precursors (from Nozaki 2001) and final state of impurities embedded in limestone (our REE data) is surprisingly close to the simplest approximation $\sim 1/\sqrt{\tau}$ ($\tau =$ mean seawater residence time for each REE; Nozaki 2001); only the unstable Ce concentrations are usually three times lower. Although we are aware of the fact that this approach is no doubt an excessive simplification (e.g. in comparison with complex and often competing processes related to organic matter, oxides, etc.; Leleyter et al. 1999), the basic information that is necessary for discrimination of various inputs seems to be involved.

The comparison of our REE data fields with the theoretical template curves for different inputs suggests that the prevailing amount of our limestone impurities may correspond to atmospheric dust (the entire section; Fig. 9a). In the Givetian part of the section, the correlations between the REE of individual samples and templates for the four types of inputs show that there is also another strong correlation for seawater solutes (Fig. 9b). The correlations for atmospheric and seawater templates are dominant (varying between −0.2 and 0.9, with a sum ~0.7), whereas the relationships to riverine and remineralization patterns are slight. If the correlation values are compared with the NGR–MS curves, it is evident that the impurities related to seawater solutes are mostly in the broad lows in these curves (= purest limestone), whereas those related to atmospheric dust mark the peaks (Gersl and Hladil 2004b). This fact can be explained by increased input of this dust in combination with more intense and direct embedding of this particulate matter in carbonates of intertidal mudflats.

Relative excess of potassium

An interesting feature of geochemical composition, based on sample analytical data, is an equal predominance of Fe, K and Al, each of these elements ~0.1 wt%. However, this K/Al ~1.0 is much higher than normal values for the dust and riverine inputs with silt and clay that typically ranges between ~0.3 and ~0.6 (e.g. Turekian and Wedepohl 1961; France-Lanord and Derry 1997; Wehausen and Brumsack 1999—cf. also K/Al for the upper Earth crust ~0.3, white mica ~0.48 or illite ~0.67). The excess of K was found in the Devonian limestones of Moravian Karst many years ago (J. Jarka, unpublished), but this fact was not fully appreciated. These excessive concentrations are even stronger with thick impurities (high NGR–MS values), and it is linked also to increased K/Na ratio (~20, max 85). The K/Al values ≥0.8 are usually linked to euxinic basins, but the Devonian, especially U. Devonian examples from limestones are more common than in other systems (e.g. Fan et al. 2004; Tribovillard et al. 2004).

There are several mechanisms potentially involved in the formation of these "hyper-potassic" complex impurities. (1) The first mechanism consists in eustatic fluctuations where, during the sea-level low stands, the largest amounts of dust were deposited on the shallowest platform surfaces. Under these conditions, long recycling of material may be considered as a possible cause (washing, colloidization, bacterial mats, moistening /desiccation, crystallization, K-enrichment mediated by phosphates, etc.). (2) The second possibility is that of massive airborne dust falling in water, causing certain fertilization and oxygen depletion, started release of reactive K, Si which could be microbially bioprecipitated. Together with the long-term interaction with sea-water itself it can probably explain the origin of K-rich suspensions, although it was documented in different ocean surface situations, e.g. in outlying areas of big river deltas (Sholkovitz and Price 1980; Michalopoulos and Aller 2004). (3) Other possibility is that Middle Devonian dried basins with evaporites provided more K, Mg, carnallite-sylvite-kainite that was assembled in Fe-rich clayey microparticles and transported with the dust plumes, e.g. Prairie Formation W Canada (Horita et al. 2002). This is a very plausible explanation. (4) Last, but not the least, we must mention the common process of formation of K-rich clays with increased depth of burial (e.g. Sayles and Mangelsdorf 1977). However, the factual variations of these processes and their effects on limestones of this platform are still unknown and need further studies.

The mineralogical aspects of K excess were solved by means of X-ray mapping, EMP and PIXE sections. A relative excess of K was found in micrometric locations of the calcite–quartz–illite/mica networks, in small 1–5 μm psilomelane spots (Mn:Ba ~2:1), and relevant points seem to be finely dispersed in microsparitic calcites around. In spite of this scatter, there still remains a close linkage of K to Fe (and the compact group of lithophile elements; Fig. 8). The elements weakly corre-

lating to this group are early and late carbonate builders Sr and Mg (~0.1) but also biophile Cd (~0.0) and V (~ −0.1). Several couples have negative correlations: e.g. Mg–Sr (−0.51), Al–Sr (−0.21), U–Mg, Y–V (−0.17), and also Be–Sr (−0.15). The ratios like those for Hf/V, K/Ba or Al/Sr show dynamic relationships among typical impurity-related elements and those of very different affinities. These independent variations of elements like Ba, Mg and V give constraints on different local aspects of environment or diagenesis (anoxia, evaporation or organic matter).

Carbon and oxygen isotopes

The fluctuation of C and O isotope (carbonate) values in this section has complex control that corresponds rather to local sea-level fluctuations and facies structure than directly to amounts of impurities in limestones. The upper beds of Givetian cycles have slightly enhanced concentrations of ^{13}C (positive shift in δ-values) versus reduced ^{18}O (negative shift). This feature (Fig. 7; right) has already been described on materials collected from the entire Moravian Karst as the so-called "mushroom-on-mushroom cycle-related pattern of platform limestones" (Hladil and Hladikova 2000). Formulation of relevant hypothesis is relatively easy because the gradually emerging reef bank was more and more affected by growing and dying algae and bacteria, and the thinnest layers of water had to have the highest temperatures and when they were emerged for some time they had also to be exposed to rainwater (vadose silts, tiny skeletal and microgeode-like quartz formations, etc.).

Anomalous detrital and impact-related admixtures

Among other accessories, two assemblages of mineral microparticles are present: the first consists detrital quartz, micas and feldspars, "fresh" rutiles and titanites + rutiles (2–6 μm) so that it corresponds to extensive and deep early Paleozoic denudation of Neoproterozoic granitoids in neighbourhood (Finger et al. 2000) and similarly also worldwide (e.g. Liegeois et al. 2003). The second is characterized by very exotic unweathered minerals (such as 8–16 μm elongated chips of +/- dozyite-like compositions with Mg:Si:Al ~ 19:13:6, no Fe; or very enigmatic Zr, Si-rich ~2–6 μm objects of icosahedron crystal shapes). The latter icosahedral shapes (Fig. 5b) are very rare in inorganic world and may require extremely high pressures, high temperatures and vapour conditions (e.g. artificial diamonds—Mani and Sunkara 2003). The Josefov-Barova-21 anomaly has also more than 10× higher concentrations of Sc, Ni and Cr, in comparison with the background values. Also the very pronounced spikes in NGR–MS are indicative of possible impact (Figs. 2, 3).

Possible significance of the section for interregional high-resolution stratigraphic correlation

Principles and current experience

The combination of four logs (MS and GRS for K, U and Th) made on relatively continuously aggraded successions of carbonate-platform strata seems to have interestingly non-random characteristics (Gersl and Hladil 2004a) which have currently proved to be effective in high-resolution regional stratigraphic correlations of the Middle Frasnian sections bridging the distances of several hundreds of kilometres among Brno, Hranice and Kielce. It is surely interesting that only a few of the complex impurity bands or peaks in the entire section can display similar or identical structures. The singularity of these stratigraphical segments is an important feature which is not limited only to one basin. If the different GRS–MS segments are developed imperfectly or with damage by local hiatuses, then the succession of underlying and overlying patterns can help with the determination. It is true, of course, unless the bias from local sedimentary conditions is not very high. The size of the characteristic windows that can be successfully correlated is usually equal to +/- 1 conodont zone. A necessary precondition is to have solid biostratigraphical markers (Crick et al. 1994; 2001; 2002), but the GRS–MS logging usually leads to better specification of correlation levels than the biostratigraphy, and the resolution greatly increases, usually ×10 to ×1000. It depends on the quality of the sections and distances among them.

The rhythms and quantities of impurity banding have usually greater-than-local consequences. It is easy demonstrable on the basis of lithological columns or outcrop photographs of *Amphipora* limestones (e.g. Zukalova 1971; Gersl and Hladil 2004a) that the GRS–MS-detected changes in amounts and quality of radioactive and magnetic impurities show modest relationships to facies and bedding characteristics of these limestones. We can find a different succession of strata (e.g. in the above-mentioned area near the town of Hranice, NE Moravia), but the stratigraphic GRS–MS structure is nearly identical to this basic section. Of course, the most general imprints of eustatic cyclicity and stratigraphic facies structure are inherited there and must be considered for the major characteristics (e.g. based on MS; da Silva and Boulvain 2005).

The nearly symmetrical NGR–MS intervals (at 130, 213 or 247 m, for example; see Figs. 2, 3) are comparable to Poisson-shape records of strong cyclic changes that are believed to result from flux of impurities (Schwarzacher 2000). The other situation, which is the opposite extreme to such completely recorded ideal cycles, is that of the abruptly inserted spikes with gradual decreasing above (at 257 m, for example). It was documented at the upper boundaries of shallowing-upward cycles (Pawellek and Aigner 2003), and such examples are not rare in well logs from any carbonate platform/

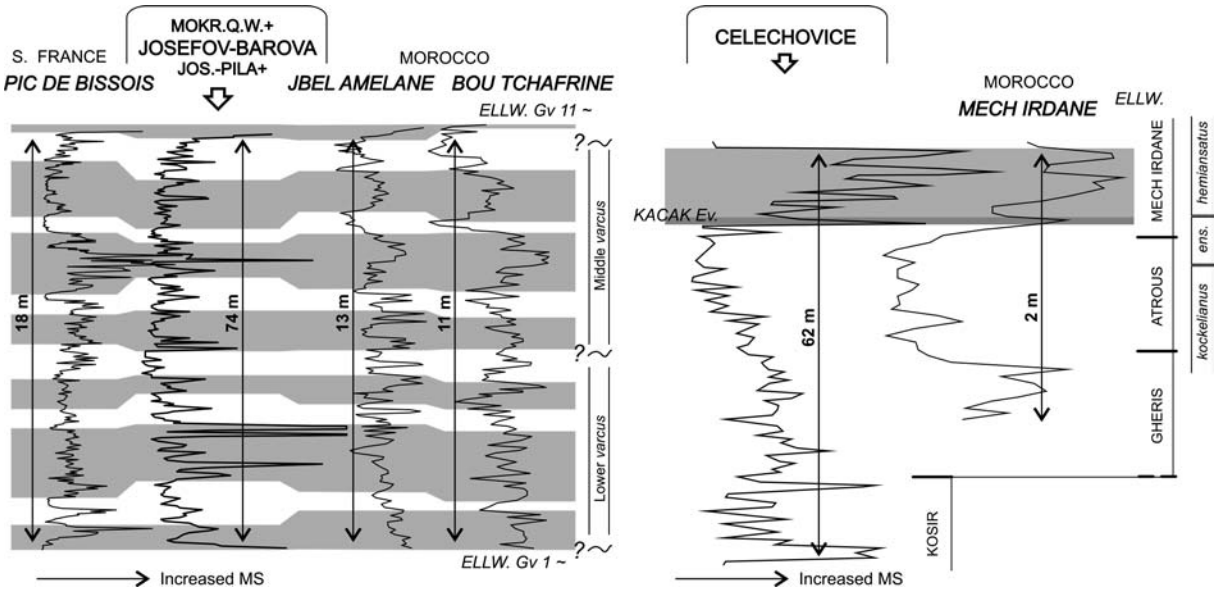

Fig. 10 Possible juxtaposition of MS sections from different basins and areas of the world; collection of segments normalized to local average values—no scale for variation. The mid-Givetian and Kacak segments of the Moravian Karst section (carbonate platform) and French and Moroccan sections (slope to pelagic systems) are compared according to the succession of tentative patterns that are assigned to segments of the sections (connected by *grey* and *white stripes*). The digital shape data from latter sections were kindly provided by B.B. Ellwood (numbers and names of MS zones—Hladil et al. 2002; Ellwood et al. 2004)

ramp systems. It corresponds to a combination of impurity flux and rate of carbonate accumulation (e.g. based on MS; Ellwood et al. 2000).

The major NGR–MS intensity fluctuations (Figs. 2, 3) occurred with the post-Kacak instabilities in environmental conditions (~ lowermost part of Lower *varcus* Zone) and to a lesser extent the Josefov-Barova-21 (at 90 m mark; ~ upper part of this zone). Higher in the section, the Lower–Middle Frasnian segment is preceded and ended by apparent nodes with high-oscillation amplitudes, which are the *disparilis–falsiovalis*? interval of terminating Givetian and the Upper *hassi* regressional interval of the late mid-Frasnian, respectively (at ~180 and 235 m marks). The relatively wild GRS–MS structure in Upp. Frasnian was probably caused by the "pre-crisis stepwise collapses" of main calcium-carbonate producers (Walliser et al. 1988; Schindler 1990) that led to increased variability in accumulation rates, recycling of the sediment, quality of surfaces embedding the impurities and many other related parameters (Copper 2001).

Perspectives of the GRS–MS correlation

There are practically no current examples of interregional GRS–MS correlations in platform limestones (with exception for unpublished materials on correlations among Czechia, Poland and Belgium—J.H.), although MS-stratigraphy shows the existence of plausible examples where very distant areas of the world were successfully correlated (e.g. Crick et al. 1997; Hladil et al. 2002; Ellwood et al. 2003). For example, an extreme lowering of MS in *kockelianus-ensensis* interval (Atrous MS Zone) was broadly correlated from peri-Gondwanan basins of Morocco, South France and Barrandian to peri-Laurussian (Rhenish) Moravia (Celechovice). And it is obvious that successions of strata and facies are very different in each of these separate basins. However, the possible perspectives to develop this sort of correlations can even be derived from the juxtaposition of the MS sections from different distant places of the world (Ellwood et al. 2004; Fig. 10 herein).

As an end note to these paragraphs about stratigraphic correlations, we would like to briefly mention one specific matter about major geo-events. The normal mode of sedimentation in carbonate sedimentary systems on platforms and adjacent ocean slopes is when the high MS values are synchronized with large-scale sea-level lowstands (e.g. Ellwood et al. 2000). But the events of Chotec, Kacak or Upper Kellwasser magnitudes have settings that are completely inverse to this commonly accepted principle. Although the NGR–MS increase with close post-event floodings seems to be realizable (these beds are often blackish-grey), mainly the pre-event association of sea-level fall and attenuation of impurities in limestones (e.g. Hladil et al. 2000) is not fully understood yet.

Discussion

Climatic conditions

The climate change impact on impurities and their GRS–MS characteristics is surely worthy of discussion.

The evolution of Devonian climates was recently reviewed and assessed by several authors (e.g. Streel et al. 2000; Copper and Scotese 2003; Royer et al. 2004), and the conclusions drawn from them suggest that the an extreme warming of Earth's surface culminated during the Givetian (to Frasnian?), when the global average temperatures increased up to +26 ± 4 °C (vs. today's ~15 °C), the high sea-level stands caused that marine flooding extended far over the continental lowlands, and all this with extremely high CO_2 atmospheric concentrations of ~0.4 wt% (vs. today's ~0.037 wt%). The Givetian land plant spores reached their maximum taxonomic diversity of all Devonian times, and also small islands in NE Moravia were likely covered by this vegetation (Purkynova et al. 2004). The high level of humidity has many evidences (e.g. pedogenic carbonates—Williams and Krause 1998; meteoric pendant cements—Hladil 1994; river deltas and vertisols in foothill catchments—Woodrow 1985), but it must be considered in conjunction with the evidences of evaporitic plains, semi-arid deserts and continental redbeds worldwide (Scotese 2005).

Extension of these aridic conditions repeatedly affected the platform on Brunnia during the period after the Middle Givetian and before Upper Frasnian (e.g. increased eolian input between the ~165 and 235 m marks of the section). The reversal of overall sea-level rise took place not earlier than with the Upper *hassi* Z. It was linked to the lowering of average temperatures and reduced plant diversity (as early as during Late Frasnian; Streel et al. 2000). The Late Frasnian increase in humidity culminated in the formation of coal rainforests in Arctic Canada and S China (Scotese 2005). The Famennian concentrations of CO_2 were already decreased by a factor of 10. Also in Moravia, the Upper Frasnian limestones above the ~235 m mark yielded rare but undoubted riverine detrital particles and rarely also ferriferous ooids (Hladil 2002). According to rough image of global climatic changes together with fragmentary evidence from the section (Fig. 2), we can be quite sure that moderately rising Th/U values can be considered as solid indicators of certain, albeit limited, riverine detrital inputs on a platform mostly surrounded by ocean sea ways. Generalizing further, we can roughly assume that the Givetian conditions on continents were affected by a combination of hot evaporitic plains and expanding vegetation covers so that detrital sources were partly covered, and the Early–Middle Frasnian was a period of more uniform and oxidic climates with extension of river plains and unconsolidated surfaces. Such an approximation may be considered in order to support an explanation of the Frasnian HM features (Fig. 3, right).

And finally, here is a short note about cyclostratigraphic analyses because many attempts were made to trace Milankovitch cycles in Devonian (e.g. House 1995; Olsen 1990; Cotter 2000; Crick et al. 2001). Fundamentally, the correct analyses need uninterrupted linear time series (even though wavelet analysis can slightly reduce this requirement; Prokoph and Barthelmes 1996). But irregularities in rates of accretion, hiatuses and differential compaction of rocks are always critical (Westphal and Boehm 2004). Also the principles how these orbital forcing mechanisms could control sea-level fluctuations in hot mid-Devonian (basically without any glaciers) are problematic, especially if compared with large magnitudes of tectono-eustatic pulses (e.g. Racki 1998).

Significance of atmospheric dust deposition

The all varieties of atmospheric dust and aerosol with that part which was drowned or dissolved in seawater compose a significant part of deposition flux on the Earth (Mahowald et al. 1999; Derbyshire 2003). The deposition of this atmospheric dust is best recognizable when this material cumulates in areas of overall sedimentary starvation or is embedded in relatively "independently" accumulated media (ice or pure carbonates, for example). The impurity systems of reef banks can, of course, record also distant effects of riverine sediment-rich flood plumes (e.g. Ba uptake by corals on the Great Barrier Reef; Alibert et al. 2003; McGulloch et al. 2003) or proximal input of detrital clays (e.g. M. Devonian of Ardennes; Chamley et al. 1997). Embedding of the beach, riverine and recycled particles are generally possible elsewhere along with deposition of non-marine/marine clastic wedges (mixed siliciclastic-carbonate sediments). However, the riverine inputs on ocean reef banks are slight. It is because of the fact that grains larger than ~5 μm are easy falling down and also the smaller particles are mostly soon removed from the upper ocean layer by biogenic particles (Honjo 1982).

In the most recent conditions, there are well-known examples of embedding of long-transported dust into the platform limestones—e.g. the case of African dust settled on Bermuda or Bahama islands. The magnitude of atmospheric flux is usually exemplified by the North American continent which has three times higher annual deposition than the emission (Ginoux et al. 2004). The calculations based on recent reviews about deposition of eolian dust and aerosols (Bory et al. 2002; Harrison et al. 2001; Mahowald et al. 1999; Tegen and Fung 1995; Duce and Tindale 1991) suggest that open ocean carbonate platforms influenced by interregional dust plumes may have a great supply of these eolian deposits, which fluctuates in long-term averages from 1.5×10^{-10} to 1.5×10^{-9} kg m^{-2} s^{-1} (= ~5–50 tons per square metre and million of years). Even if we reduce these amounts by 50–75%, according to possible washing and dissolution, it is still a significant concentration of impurity in limestone that ranges between 2.5 and 25 wt% in case a 20 m/Ma average rate of carbonate accumulation (Hladil et al. 2003a). These quantities warn us that these eolian inputs in shallow-water reef banks may be of equal, if not greater importance than the normal detrital inputs.

Conclusions

The shallowest pure carbonate environments on the ocean-fringed and continuously subsiding/accreting carbonate platform, with large distance from the river mouths (clastic wedges none or much reduced), offer an excellent opportunity to analyse the impurity fluxes that can be significantly, although not exclusively, related to atmospheric dust. The composite section in the Devonian, mid-Eifelian to end-Frasnian limestones of Moravian Karst contains the non-carbonate complex impurities which comprise mainly the very fine particulate smectite–illite(mica) material that is combined with significant amounts iron oxides (mostly goethite, hematite). These impurities contain the REE characteristics that are significantly associated with interregional eolian inputs. There is also a high preponderance of U over Th. Because of the fact that this feature is practically unrelated to possible euxinic conditions, it gives further evidence to the debate about predominant eolian input characteristics. These assumptions about increased proportion of atmospheric dust deposits embedded in limestones may explain the long distance MS (and GRS–MS) stratigraphic correlations that bridge various basins and carbonate facies. The principal contribution of this paper is the presentation of the GRS–MS data from a long-composed section that can further serve as the basis for high-resolution stratigraphic correlation.

ESM1

Electronic Supplementary Material 1, background dataset on-line: Hladil-ESM1.xls. The Middle Eifelian to Upper Frasnian composite Section of the Moravian Karst, Czech Republic. Natural gamma-ray (NGR and GRS) and magnetic susceptibility (MS) values of platform limestones: spreadsheets with numerical ''raw'' data, with spacing 0.5 m.

Acknowledgments Project: AVOZ30130516 ''Earth Systems''. Consulting and support: X-ray diffractometry—K. Melka (Inst. Geol. ASCR); PIXE probing—J. Voltr (Phys. Electronics, Czech Tech. Univ.); magnetism—M. Krs, P. Pruner and M. Chadima (Paleomag. Lab. Pruhonice), B.B. Ellwood (Dept. Geol. Geophys., Louisiana State Univ.), F. Hrouda (Agico Ltd.); gamma-ray—I. Kasparec (Exploranium CZ). Particular indebtedness is due to helpful comments and corrections by journal referees.

References

Alibert C, Kinsley L, Fallon SJ, McCulloch MT, Birkelmans R, McAllister F (2003) Source of trace element variability in the Great Barrier Reef corals affected by the Burdekin flood plumes. Geochim Cosmochim Acta 67:231–246

Babek O (1996) Thinning and fining-upward megasequences in Middle Devonian carbonate slope deposits, Moravia, Czech Republic. Neues Jahrb Geol Palaeont Abh 202:409–432

Bond D, Zaton M (2003) Gamma-ray spectrometry across the Upper Devonian basin succession at Kowala in the Holy Cross Mountains (Poland). Acta Geol Polon 53:93–99

Bory A, Dulac F, Moulin C, Chiapello I, Newton PP, Guelle W, Lambert CE, Bergametti G (2002) Atmospheric and oceanic dust fluxes in the northeastern tropical Atlantic Ocean: how close a coupling? Ann Geophys 20:2067–2076

Bosak P, Mylroie JE, Hladil J, Carew JL, Slavik L (2002) Blow Hole Cave. An unroofed cave on San Salvador Island, the Bahamas, and its importance for detection of paleokarst caves on fossil carbonate platforms. Acta Carsol 31:51–74

Chamley H, Proust JN, Mansy JL, Boulvain F (1997) Diagenetic and palaeogeographic significance of clay, carbonate and other sedimentary components in the middle Devonian limestones of western Ardenne, France. Palaeogeogr Palaeoclimatol Palaeoecol 129:369–385

Collinson DW (1983) Methods in rock magnetism and palaeomagnetism: techniques and instrumentations. Chapman and Hall, London, p 503

Copper P (2001) Reef development at the Frasnian/Famennian mass extinction boundary. Palaeogeogr Palaeoclimatol Palaeoecol 181:27–65

Copper P, Scotese C (2003) Megareefs in mid-Devonian supergreenhouse climates. In: Chan MA, Archer AW (eds) Extreme depositional environments: mega end members in geologic time. Geol Soc Am Spec Pap 370:209–230

Cotter E (2000) Depositional setting and cyclic development of the lower part of the Witteberg Group (Mid- to Upper Devonian), Cape Supergroup, Western Cape, South Africa. South Afr J Geol 103:1–14

Crick RE, Ellwood BB, El Hassani A (1994) Integration of biostratigraphy, magnetic susceptibility and relative sea-level change: a new look at high resolution correlation. SDS Newslett 11:59–66

Crick RE, Ellwood BB, El Hassani A, Feist R, Hladil J (1997) Magnetosusceptibility event and cyclostratigraphy (MSEC) of the Eifelian-Givetian GSSP and associated boundary sequences in North Africa and Europe. Episodes 20:167–175

Crick RE, Ellwood BB, Hladil J, El Hassani A, Hrouda F, Chlupac I (2001) Magnetostratigraphy susceptibility of the Pridolian-Lochkovian (Silurian-Devonian) GSSP (Klonk, Czech Republic) and a coeval sequence in Anti-Atlas, Morocco. Palaeogeogr Palaeoclimatol Palaeoecol 167:73–100

Crick RE, Ellwood BB, Feist R, El Hassani A, Schindler E, Dreesen R, Over DJ, Girard C (2002) Magnetostratigraphy susceptibility of the Frasnian/Famennian boundary. Palaeogeogr Palaeoclimatol Palaeoecol 181:67–90

da Silva C, Boulvain F (2002) Sedimentology, magnetic susceptibility and isotopes of a Middle Frasnian carbonate platform: Tailfer section, Belgium. Facies 46:89–102

da Silva C, Boulvain F (2003) Sedimentology, magnetic susceptibility and correlations of Middle Frasnian platform limestone (Tailfer and Aywaille sections, Belgium). Geologica Belgica 6:81–96

da Silva C, Boulvain F (2005) Upper Devonian carbonate platform correlations and sea level variations recorded in magnetic susceptibility. Palaeogeogr Palaeoclimatol Palaeoecol, in press

Derbyshire E (2003) Loess, and the dust indicators and records of terrestrial and marine palaeoenvironments (DIRTMAP) database. Q Sci Rev 22:1813–1819

Doriguetto AC, Goulart AT, de Jesus Filho MF, Fabris JD, Santana GP (1998) Ilmenite in soil forming from Brazilian amphibolite. Eur J Soil Sci 49:541–545

Duce RA, Tindale NW (1991) Atmospheric transport of iron and its deposition in the ocean. Limnol Oceanogr 36:1715–1726

Dunlop DJ, Ozdemir O (1997) Rock magnetism. Cambridge University Press, London, p 573

Ellwood BB, Crick RE, El Hassani A, Benoist SL, Young RH (2000) Magnetosusceptibility event and cyclostratigraphy (MSEC) in marine rocks and the question of detrital input versus carbonate productivity. Geology 28:1135–1138

Ellwood BB, Benoist SL, El Hassani A, Wheeler C, Crick RE (2003) Impact ejecta layer from the mid-Devonian: possible connection to global mass extinctions. Science 300:1734–1737

Ellwood BB, Benoist SL, El Hassani A, Feist R (2004) High resolution correlation using graphic correlation of biostratigraphic and magneto-stratigraphic or chemostratigraphic data sets: illustrating the method by defining the Middle Devonian magnetostratigraphic susceptibility for sections from France and Morocco. Abstr SDS 2004 Meet Rabat, Morocco:P8

Fan D, Zhang T, Ye J (2004) The Xikuangshan Sb deposit hosted by the Upper Devonian black shale series, Hunan, China. Ore Geol Rev 24:121–133

Finger F, Tichomirowa M, Pin C, Hanzl P (2000) Relics of an early-Panafrican metabasite-metarhyolite formation in the Brno Massif, Moravia, Czech Republic. Int J Earth Sci 89:328–335

France-Lanord C, Derry LA (1997) Organic carbon burial forcing of the carbon cycle from Himalayan erosion. Nature 390:65–67

Galle A, Friakova O, Hladil J, Kalvoda J, Krejci Z, Zukalova V (1988) Biostratigraphy of Middle and Upper Devonian carbonates of Moravia, Czechoslovakia. Can Soc Petrol Geol Mem 14:633–645

Galle A, Hladil J (1991) Lower Paleozoic corals of Bohemia and Moravia. In: 6th international symposium on Fossil Cnidaria and Porifera. Fossil Cnidaria, Munster, Guidebook B3, pp 1–83

Gersl M, Hladil J (2004a) Gamma-ray and magnetic susceptibility correlation across Frasnian carbonate platform and search for the "punctata" equivalents in stromatoporoid-coral limestone facies of Moravia. Geol Q 48:283–292

Gersl M, Hladil J (2004b) Weathering products trapped in pure platform limestones: geochemical picture of magnetic susceptibility and gamma-ray variations. Geochim Cosmochim Acta 68(Suppl 11):A446 post 4.5.P25

Gilmore G, Hemingway JD (1995) Practical gamma-ray spectrometry. Wiley, p 322

Goulard AT, de Jesus Filho MF, Fabris JD, Coey JMD (1994) Characterization of soil ilmenite developed from basalt. Hyperfine Interact 91:771–775

Harrison SP, Kohfeld KE, Roelandt C, Claquin T (2001) The role of dust in climate changes today, at the last glacial maximum and in the future. Earth-Sci Rev 54:43–80

Hladil J (1983) The biofacies section of Devonian limestones in the central part of the Moravian Karst. Sbor Geol Ved Geol Prague 38:71–94

Hladil J (1994) Microfacies of the Devonian limestones in Moravia, Part II, Overview of microfacies. Zem Plyn Nafta Gbely 39:19–70

Hladil J (2002) Geophysical records of dispersed weathering products on the Frasnian carbonate platform and early Famennian ramps in Moravia, Czech Republic: proxies for eustasy and palaeoclimate. Palaeogeogr Palaeoclimatol Palaeoecol 181:213–250

Hladil J (2003) Devonian and Carboniferous of the Moravian Karst. In: 9th international symposium on Fossil Cnidaria and Porifera. Graz-Brno, Field Trip Guidebook B2, p 15 http://home.gli.cas.cz/hladil/www/B2-Guidebook-MK.pdf

Hladil J, Hladikova J (2000) Isotopic compositions of carbon and oxygen in platform/reef carbonates of the Moravian Karst. In: Oschmann W, Steininger F, Fursich FT (eds) Biomarkers and stable isotopes in palaeontology. Eur Palaeont Assoc Workshop Frankfurt 2000:51–53

Hladil J, Patocka F, Kachlik V, Melichar R, Hubacik M. (2003a) Metamorphosed carbonates of Krkonose Mountains and Paleozoic evolution of Sudetic tarranes (NE Bohemia, Czech Republic). Geol Carpath 54:281–297

Hladil J, Bosak P, Slavik L, Carew JL, Mylroie JE, Gersl M (2003b) Early diagenetic origin and persistence of gamma-ray and magnetosusceptibility patterns in platform carbonates: comparison of Devonian and Quaternary sections. Phys Chem Earth 28:719–727

Hladil J, Gersl M, Hladikova J, Frana J (2004) Environmental disturbances in early Middle Frasnian (punctata Zone)—Alamo Comet was likely accompanied by other bolides. Acad Sci CR Inst Geol Ann Rep 2003:46–47

Hladil J, Pruner P, Venhodova D, Hladilova T, Man O (2002) Toward an exact age of Middle Devonian Celechovice corals—past problems in biostratigraphy and present solutions complemented by new magnetosusceptibility measurements. Coral Res Bull 7:65–71

Honjo S (1982) Seasonality of biogenic and lithogenic fluxes in the Panama Basin. Science 218: 883–884

Horita J, Zimmermann H, Holland HD (2002) Chemical evolution of seawater during the Phanerozoic: Implications from the record of marine evaporites. Geochim Cosmochim Acta 66:3733–3756

Kao SJ, Horng CS, Roberts AP, Liu KK (2004) Carbon-sulfur-iron relationships in sedimentary rocks from southwestern Taiwan: influence of geochemical environment on greigite and pyrrhotite formation. Chemical Geology 203:153–168

Krs M, Pruner P, Man O (2001) Tectonic and paleogeographic interpretation of the paleomagnetism of Variscan and pre-Variscan formations of the Bohemian Massif, with special reference to the Barrandian terrane. Tectonophysics 332:93–114

Leleyter L, Probst JL, Depetris P, Haida S, Mortatti J, Rouault R, Samuel J (1999) REE distribution pattern in river sediments: partitioning into residual and labile fractions. Compt Rend Acad Sci Ser IIA 329:45–52

Lennie AR, Redfern SAT, Champness PE, Stoddart CP, Schofield PF, Vaughan DJ (1997): Transformation of mackinawite to greigite: and in situ X-ray powder diffraction and transmission electron microscope study. Am Mineral 82:302–309

Liegeois JP, Latouche L, Boughrara M, Navez J, Guiraud M (2003) The LATEA metacraton (Central Hoggar, Tuareg shield, Algeria): behaviour of an old passive margin during the Pan-African orogeny. J Afr Earth Sci 37:161–190

Lo Monaco S, Lopez L, Rojas H, Garcia D, Premovic P, Briceno H (2002) Distribution of major and trace elements in La Luna Formation, Southwestern Venezuelan Basin. Organic Geochem 33:1593–1608

Luening S, Wendt J, Belka Z, Kaufmann B (2004) Temporal–spatial reconstruction of the early Frasnian (Late Devonian) anoxia in NW Africa: new field data from the Ahnet Basin (Algeria). Sedim Geol 163: 237–264

Mahowald N, Kohfeld K, Hansson M, Balkanski Y, Harrison SP, Prentice IC, Schulz M, Rodhe H (1999) Dust sources and deposition during the last glacial maximum and current climate: a comparison of model results with paleodata from ice cores and marine sediments. J Geophys Res 104:15895–15916

Mani RC, Sunkara MK (2003) Kinetic faceting of multiply twinned diamond crystals during vapor phase synthesis. Diam Rel Mater 12:324–329

Marx SK, Kamber BS, McGowan HA (2005) Provenance of long travelled dust determined with ultra trace element composition: a pilot study with samples from New Zealand glaciers. Earth Surf Processes Landforms, (in press)

McCulloch M, Fallon SR, Wyndham T, Hendy E, Lough J, Barnes D (2003) Coral record of increased sediment flux to the inner Great Barrier Reef since European settlement. Nature 421(6924):727–730

Michalopoulos P, Aller RC (2004) Early diagenesis of biogenic silica in the Amazon delta: Alteration, authigenic clay formation, and storage. Geochim Cosmochim Acta 68:1061–1085

Nozaki Y (2001) Rare earth elements and their isotopes. In: Steele JS, Turekian KK, Thorpe SA (eds) Encyclopedia of Ocean sciences. Academic, London, pp 2354–2366

Olsen H (1990) Astronomical forcing of meandering river behaviour: Milankovitch cycles in Devonian of East Greenland. Paleogeogr Paleoclimatol Paleoecol 79:99–115

Pawellek T, Aigner T (2003) Stratigraphic architecture and gamma ray logs of deeper ramp carbonates (Upper Jurassic, SW Germany). Sed Geol 159:203–240

Plank T, Langmuir CH (1998) The geochemical composition of subducting sediment and its consequences for the crust and mantle. Chem Geol 145:325–394

Prokoph A, Barthelmes F (1996) Detection of non-stationarities in geological time-series. Wavelet-analysis of chaotic and cyclic sequences. Comput Geosci 22:1097–1108

Purkynova E, Gilikova H, Jachowitz M, Filipiak P (2004) Paleobotanical records from basal Devonian clastics in Menin and Kozlovice boreholes, Moravia, Czech Republic. Cas Slez Muz Opava A 53:193–204

Racki G (1998) Frasnian-Famennian biotic crisis: undervalued tectonic control? Palaeogeogr Palaeoclimatol Palaeoecol 141:177–198

Racki G, Piechota A, Bond D, Wignall PB (2004) Geochemical and ecological aspects of lower Frasnian pyrite-goniatite level at Kostomloty (Holy Cross Mountains, Central Poland). Geol Quart 48:267–282

Richter C, Valet JP, Solheid PA (1997) Rock-magnetic properties of sediments from Ceara Rise (Site 929), and implications for the origin of their magnetic susceptibility. In: Shackleton NJ, Curry WB, Richter C, Bralower TJ (eds) Proceedings of ODP, Scientific Results, vol 154, pp 169–179

Royer DL, Berner BA, Montanez IP, Tabor NJ, Beerling DJ (2004) CO_2 as a primary driver of Phanerozoic climate. GSA Today 14(3):4–10

Ruffell A, Worden R (2000) Palaeoclimate analysis using spectral γ-ray data from the Aptian (Cretaceous) of southern England and southern France. Palaeogeogr Palaeoclimatol Palaeoecol 155:265–283

Sayles FL, Mangelsdorf PC (1977) The equilibrium of clay minerals with seawater: exchange reactions. Geochim Cosmochim Acta 41:951–960

Schindler E (1990) Die Kellwasser-Krise (hohe Frasne-Stufe, Ober-Devon). Gott Arb Geol Palaont 46:1–115

Schwarzacher W (2000) Repetitions and cycles in stratigraphy. Earth Sci Rev 50:51–75

Scotese CR (2005) Paleomap project, climate history. http://www.scotese.com/paleocli.htm

Sholkovitz ER, Price NB (1980) The major-element chemistry of suspended matter in the Amazon Estuary. Geochim Cosmochim Acta 44:163–171

Slavik L, Hladil J, Blazek R, Kruta T (2000) Anatomy of the Pragian stratigraphic column; gamma-ray spectrometric record throughout a complete 170-m thick Pragian section in calciturbidite/hemipelagite facies. Subcomm Devon Stratigr Newsl 17:46–47

Smalley IJ, Kumar R, O'Hara Dhand K, Jefferson IF (2004) The formation of quartz silt for terrestrial sediments: particularly loess deposits. Int. Workshop Particle Size Sed. Dynamics. Hanse-Wissenschaftskol Delmenhorst 2004:129–130

Streel M, Caputo MV, Loboziak S, Melo JHG (2000) Late Frasnian-Famennian climates based on palynomorph analyses and the question of the Late Devonian glaciations. Earth Sci Rev 52:121–173

Tegen I, Fung I (1995) Contribution to the atmospheric mineral aerosol load from land surface modification. J Geophys Res 100:18707–18726

Tribovillard N, Averbuch O, Devleeschouwer X, Racki G, Riboulleau A (2004) Deep-water anoxia over the Frasnian–Famennian boundary (La Serre, France): a tectonically induced oceanic anoxic event? Terra Nova 16:288–295

Turekian KK, Wedepohl KH (1961) Distribution of the elements in some major units of the earth's crust. Geol Soc Am Bull 72:175–192

Ures M, LeMenn J, Hladil J (1999) Middle Devonian crinoid columnals from Celechovice in Moravia, Czech Republic. Bull Geosci Czech Geol Surv 74:323–333

Vavrdova M, Mikulas R, Nehyba S (2003) Lower Cambrian siliciclastic sediments in Southern Moravia (Czech Republic) and their paleogeographical constraints. Geol Carpath 52:67–79

Walliser OH, Lottmann J, Schindler E (1988) Global events in the Devonian of Kellerwald and Harz Mountains. Cour Forsch-Inst Senckenberg 102:190–193

Wehausen R, Brumsack HJ (1999) Cyclic variations in the chemical composition of eastern Mediterranean Pliocene sediments: a key for understanding sapropel formation. Mar Geol 153:161–176

Wehausen R, Tian J, Brumsack HJ, Cheng X, Wang P (2003) Geochemistry of Pliocene sediments from ODP Site 1143 (southern South China Sea). In: Prell WL, Wang P, Blum P, Rea DK, Clemens SC (eds). Proceedings of ODP, scientific results vol 184, pp 1–25

Westphal H, Boehm F (2004) Orbital frequencies in the carbonate sedimentary record: distorted by diagenesis? Facies 50:3–11

Williams CA, Krause FF (1998) Pedogenic-phreatic carbonates on a Middle Devonian (Givetian) terrigenous alluvial-deltaic plain, Gilwood Member (Watt Mountain Formation), northcentral Alberta, Canada. Sedimentology 45:1105–1124

Woodrow DL (1985) Paleogeography, paleoclimate, and sedimentary processes of the Late Devonian Catskill Delta. Geol Soc Amer Spec Pap 201:51–63

Zukalova V (1971) Stromatoporoidea from the Middle and Upper Devonian of the Moravian Karst. Rozpr Ustr Ust Geol Prague 37:3–143

Zukalova V, Chlupac I (1982) Stratigraphic classification of non-metamorphosed Devonian of the Moravian-Silesian area. Cas Mineral Geol 27:225–241